JGR Oceans

RESEARCH ARTICLE
10.1029/2023JC020820

Spatially and Temporally Variable Impacts of Hurricanes on Shallow Sediment Structure

W. C. Clemo[1,2,3,4], K. M. Dorgan[3,4], D. J. Wallace[5], and B. Dzwonkowski[3,4]

[1]National Research Council Research Associateship Program, U.S. Naval Research Laboratory, Stennis Space Center, MS, USA, [2]Ocean Sciences Division, U.S. Naval Research Laboratory, Stennis Space Center, MS, USA, [3]Stokes School of Marine and Environmental Sciences, University of South Alabama, Mobile, AL, USA, [4]Dauphin Island Sea Lab, Dauphin Island, AL, USA, [5]School of Ocean Science and Engineering, University of Southern Mississippi, Stennis Space Center, MS, USA

Abstract Sediment dynamics are fundamental to understanding coastal resiliency to climate change in the coming decades. Tropical cyclones can radically alter shallow sediment properties; however, the uncertain and destructive nature of tropical cyclones make understanding and predicting their impacts on sediments challenging. Here, grain size sampling in conjunction with continuous hydrodynamic data provided an unprecedented perspective of the impacts of two tropical cyclones, including Hurricane Sally (2020), in which the inner core of the storm passed directly over the field sites, on shallow coastal sediments in Alabama (USA). Sampling directly before and after Sally as well as out to ~7 months after the second storm event, Hurricane Zeta, showed that the changes in sediments following storm events exhibited notable site-to-site variability. This variability during the first storm event was consistent with low sand supply and flow interactions driven by local bathymetry that led to sand transport and deposition at some previously-muddy sites, near-surface mud loss at some sandy sites, or little change at others. Post-Sally impacts to grain size were well preserved 8 months after the storm, despite passage of Zeta as well as seasonal winds and riverine inputs during winter and spring. Overall, high temporal-resolution sampling over a relatively large area (<500 km^2) revealed relatively small-scale spatial variability (on the order of 5–10 km) of hurricane impacts to sediment structure. These observations demonstrate a critical limitation for accurately predicting changes to coastal sediment dynamics in the face of a changing climate and its impact on tropical cyclones.

Plain Language Summary Extreme storms cause major disturbance to shallow coastal sediments, which are important for coastal resiliency to climate change. However, capturing the localized impacts of storms on sediments is difficult due to the unpredictable and destructive nature of these extreme events. We collected sediment properties and uninterrupted water flow measurements before and after two consecutive tropical cyclones: Hurricane Sally, in which the center of the storm passed directly over the field sites, and Hurricane Zeta, which passed west of the sites. These observations provided an unprecedented perspective of tropical cyclone impacts to Alabama (USA) shallow coastal sediments. Comparison of sediments collected days before and after Sally as well as over a longer-term period over ~7 months after Zeta showed that storm impacts varied considerably between sites separated by only a few kilometers. This variability is consistent with low sand supply and storm flow interacting with seafloor terrain, which funneled resuspended sand to certain sites. The apparent post-Sally sediment impacts changed little over the 8 months after the storm, providing insight on ancient storm layers preserved in the geological record. The observed spatial variability presents a challenge for predicting coastal sediment dynamics in the face of a changing climate influencing extreme storms.

Key Points:

- Hurricanes Sally and Zeta were the most intense storm events to impact coastal Alabama (USA, northern Gulf of Mexico) in over a decade
- Storm impacts on sediments showed spatial variability, likely from interactions of currents, bathymetry, and pre-storm sediments
- Apparent sediment layering and winnowing from Sally was mostly preserved, despite Zeta, winter/spring winds, and riverine inputs

Supporting Information:

Supporting Information may be found in the online version of this article.

Correspondence to:

W. C. Clemo,
william.c.clemo.ctr@us.navy.mil

Citation:

Clemo, W. C., Dorgan, K. M., Wallace, D. J., & Dzwonkowski, B. (2024). Spatially and temporally variable impacts of hurricanes on shallow sediment structure. *Journal of Geophysical Research: Oceans*, *129*, e2023JC020820. https://doi.org/10.1029/2023JC020820

Received 13 DEC 2023
Accepted 3 JUL 2024

Author Contributions:

Conceptualization: W. C. Clemo, K. M. Dorgan
Data curation: W. C. Clemo, B. Dzwonkowski
Formal analysis: W. C. Clemo, D. J. Wallace, B. Dzwonkowski
Funding acquisition: K. M. Dorgan, B. Dzwonkowski
Investigation: W. C. Clemo, K. M. Dorgan, B. Dzwonkowski
Methodology: W. C. Clemo, K. M. Dorgan, D. J. Wallace, B. Dzwonkowski
Project administration: W. C. Clemo, K. M. Dorgan
Resources: K. M. Dorgan, D. J. Wallace
Software: W. C. Clemo, D. J. Wallace, B. Dzwonkowski
Supervision: W. C. Clemo, K. M. Dorgan, D. J. Wallace
Validation: W. C. Clemo, B. Dzwonkowski

1. Introduction

Coastal barrier island systems, especially in the Gulf of Mexico, experience the combination of rapid relative sea-level rise from warming and subsidence, anthropogenic terrestrial sediment supply reduction, and frequent impacts from extreme storms (Anderson et al., 2022; FitzGerald et al., 2008; Keen et al., 2012). On the northern Gulf of Mexico coast and other storm-prone but otherwise low-energy coasts, extreme storms, despite their short duration and episodic nature, often dominate cross-shelf sediment transport and can result in permanent loss of sand from barrier island systems (Goff et al., 2010; Hayes, 1967; Keen & Slingerland, 1993; Li et al., 2015; Wallace & Anderson, 2013). Sediment loss during tropical cyclones along eroding and storm-prone

Visualization: W. C. Clemo, D. J. Wallace, B. Dzwonkowski
Writing – original draft: W. C. Clemo
Writing – review & editing: W. C. Clemo, K. M. Dorgan, D. J. Wallace, B. Dzwonkowski

coasts may be enhanced with increased storm intensity expected with climate change (Anderson et al., 2022; Emanuel, 2017).

1.1. Storm Impacts on Coastal Sediments

Substantial sediment resuspension and transport by tropical cyclones can leave behind distinct sediment layers that differ in composition from the pre-storm sediment; these layers are referred to as event or storm beds. Storm beds overlay pre-storm sediment and often consist of graded sandy layers below upwardly-fining layers of mud (Hayes, 1967; Keen et al., 2006; Morton, 1988). Alternatively, storm beds may be thick, muddy layers resulting from mud deposition after storm waves and currents have subsided and/or increased mud delivery from high river flow following heavy rainfall (Allison et al., 2005; Bentley et al., 2002; Gagan et al., 1990; Keen et al., 2012). Sandy storm beds can be used to estimate sand loss from barrier islands during extreme events (Goff et al., 2010; Hayes, 1967; Li et al., 2015; Wallace & Anderson, 2013).

Storm beds are generated by a combination of resuspension of the local sediment by waves and deposition of sediment transported by currents (Allison et al., 2005; Cong et al., 2021; Goni et al., 2007; Keen et al., 2012). Modeling of current-dominated storm flow during hurricanes Camille (1969) and Andrew (1992) showed spatially variable storm beds that were attributed to rapidly changing bottom currents that interacted with bathymetry changes. Alternatively, wave-dominated resuspension in the presence of weak currents has been demonstrated to produce relatively uniform storm beds (Bentley et al., 2002; Keen et al., 2012). Spatial variability in storm bed thickness and resuspension depth also arises from differences in distance from the storm center and water depth. While storm beds are generally thickest closest to the storm track, stronger waves and currents to the right of the storm center in the northern hemisphere usually generate more resuspension compared to the left of the storm center (Cong et al., 2021; Keen et al., 2006; Xu et al., 2016). Additionally, shallow areas near the storm center may not exhibit storm bedding due to net erosion, whereas net deposition may occur in deeper areas away from the storm track as near-bed wave orbital velocity dissipates (Cong et al., 2021; Xu et al., 2016). Sediment availability from the barrier system for transport is also an important factor in storm bed distribution and geometries (Wallace & Anderson, 2013).

Several mechanisms have been proposed to explain how storm-generated currents transport barrier island and shoreface sediment offshore to form storm bed layers. Offshore-thinning graded layers of mud over sand observed after hurricanes Carla (1961) and Ike (2008) on the Texas shelf were suggested to be deposited by turbidity currents that resulted from storm surge ebb being funneled through hurricane-cut channels in barrier islands (Goff et al., 2010; Hayes, 1967). The barrier islands impacted by these storms experienced storm surge heights of up to 6.7 m (Hayes, 1967) and 5 m (Goff et al., 2010), leading to substantial overwash, which in some cases cut new channels. An alternate explanation was that onshore storm winds drove onshore currents at the sea surface leading to offshore return of near-bed flow, and that this post-storm return flow, not storm surge ebb, was responsible for these graded sand beds (Morton, 1981; Snedden & Nummedal, 1991). Storm beds in shallower areas have also been suggested to result from direct wind-driven transport during storm passage (Keen & Slingerland, 1993; Morton, 1981).

Comparisons of modern storm beds to ancient storm beds preserved in the rock record provide important insight into ancient coastal sediment dynamics and storm frequency (Keen et al., 2012; Morton, 1988). Thick storm beds are generally uncommon in modern sediments due to a relative shortage in sediment supply characterizing the current post-glacial period of sea level rise (Allison et al., 2005; Keen et al., 2006, 2012). The northern Gulf of Mexico continental shelf, however, presents an area conducive to storm bed deposition and preservation (Balsam & Beeson, 2003; Keen et al., 2006), likely due to the combination of the prevalence of tropical cyclones in an otherwise low-energy area and predominance of heterogeneous muddy sediments, making preservation more likely and allowing easier distinction of sandy storm layers (Keen et al., 2012; Morton, 1988; Snedden & Nummedal, 1991).

Due to the unpredictable and destructive nature of extreme storms, few studies have examined a high-resolution temporal sampling of deposited storm beds while collecting hydrographic data immediately before, during and after storm passage (Corbett et al., 2014; Xu et al., 2016). Instead, studies often rely on modeling to assess storm impacts to the sediment (Bentley et al., 2002; Cong et al., 2021; Keen & Glenn, 2002; Keen & Slingerland, 1993; Snedden & Nummedal, 1991; Xu et al., 2016). However, difficulties

in simulating variable physical forcing during storms, flow-bathymetry interactions, and spatial variability and cohesive properties of pre-storm sediments can lead to large uncertainties in predicted storm bed thickness and spatial variability immediately following storm impacts (Bentley et al., 2002; Keen & Slingerland, 1993; Xu et al., 2016). Most studies of modern subtidal storm beds in the Gulf of Mexico have occurred in the northwest region on the Texas and Louisiana shelves (Hayes, 1967; Keen et al., 2012; Morton, 1988), while fewer studies have been performed in the Mississippi Bight region (between the Chandeleur Islands and the Florida panhandle, including the Alabama coast; Figure 1; but see Bentley et al., 2002; Keen et al., 2006) despite proximity to major hurricane impacts within the last 20 years in addition to high small-scale spatial and temporal variability in sediment type (Hummel & Smith, 1996). Therefore, direct sediment and hydrographic sampling of extreme storm events is important for constraining predictions of storm impacts to coastal sediments, especially in the understudied and highly erosive (Morton, 2008; Otvos & Carter, 2008) Alabama coastal sediments with generally low sand supply (Anderson et al., 2023; Hollis et al., 2019; Otvos & Carter, 2013).

An equally critical motivation concerns understanding the ultimate fate of storm deposits. Following deposition, storm beds are subject to alteration by physical and biological processes. Storm beds produced by subsequent storms may incorporate sediment from or contribute to previous storm layers, making it difficult to distinguish individual events if multiple events occur relatively close to each other (Goni et al., 2007; Keen et al., 2012). Storm beds may also be impacted by the burrowing activities of infaunal animals, which mix the top ~10 cm of sediments and blur storm bed layers over time (Boudreau, 1998; Meysman et al., 2006; Solan et al., 2019; Wheatcroft et al., 2007). Thus, better characterization of the short-term changes to modern storm beds is needed to better interpret storm beds found in the sedimentary and rock records. Overall, collecting high-resolution observations of storm impacts in vulnerable coastal environments is important for predicting the generation and preservation of storm beds.

1.2. Study Area: The Alabama Shelf

Located at the center of the Mississippi Bight, coastal Alabama provides a unique and understudied sedimentary environment in which to study tropical cyclone impacts. Coastal Alabama is microtidal (mean tidal range: 0.37 m) and has low to moderate wind and wave intensities (mean wind speed: 3.6 m s^{-1}; mean wave height: <1 m), which are generally stronger and from the north during winter and calmer and from the south during summer (Hummell, 1996). The Mobile Bay estuary forms much of coastal Alabama and empties into the Gulf of Mexico primarily through Main Pass between Dauphin Island and the Fort Morgan Peninsula (Figure 1). Dauphin Island is one of the most critically eroding barrier islands in the Gulf of Mexico (Morton, 2008; Otvos & Carter, 2008) due to very low sand supply (Hollis et al., 2019; Otvos & Carter, 2013). A distinct ebb tidal delta at the mouth of Mobile Bay extends ~10 km into the Gulf of Mexico and includes the subaerial Sand Island peninsula (Hummell, 1996). Mobile Bay receives the majority of freshwater inputs from the Alabama and Tombigbee rivers, resulting in an annual delivery of 3.25×10^6 t of sediment to the Bay and a major source of river discharge to the Gulf of Mexico, second only to the Mississippi-Atchafalaya river system (Byrnes et al., 2017; Dzwonkowski et al., 2011). River discharge into the bay peaks in late winter/early spring and reaches a minimum in late summer/early fall (Dzwonkowski et al., 2011; Stumpf et al., 1993). During high riverine inputs to Mobile Bay and/or periods of strong winds and waves, which resuspend the shallow (average depth: ~3 m) sediments (mainly clays and silty clays; Jacquot et al., 2018), large amounts of muddy sediments are transported offshore through Main Pass in a surface plume, leading to annual sediment delivery of 1–2×10^6 t to the Alabama shelf (Dinnel et al., 1990). This sediment plume is usually deflected westward due to the predominant westward longshore current and the Coriolis effect (Cipriani & Stone, 2001). However, the plume direction can be shifted during periods of strong west or south winds and/or high freshwater discharge (Dzwonkowski et al., 2015). Because of the strong riverine influence, Alabama coastal sediments are highly spatially variable, generally shifting from muds west of Main Pass to clean sands to the east (Balsam & Beeson, 2003; Hummel & Smith, 1996; Jenkins, 2011). This sedimentary heterogeneity facilitates identification of storm beds (Keen et al., 2006).

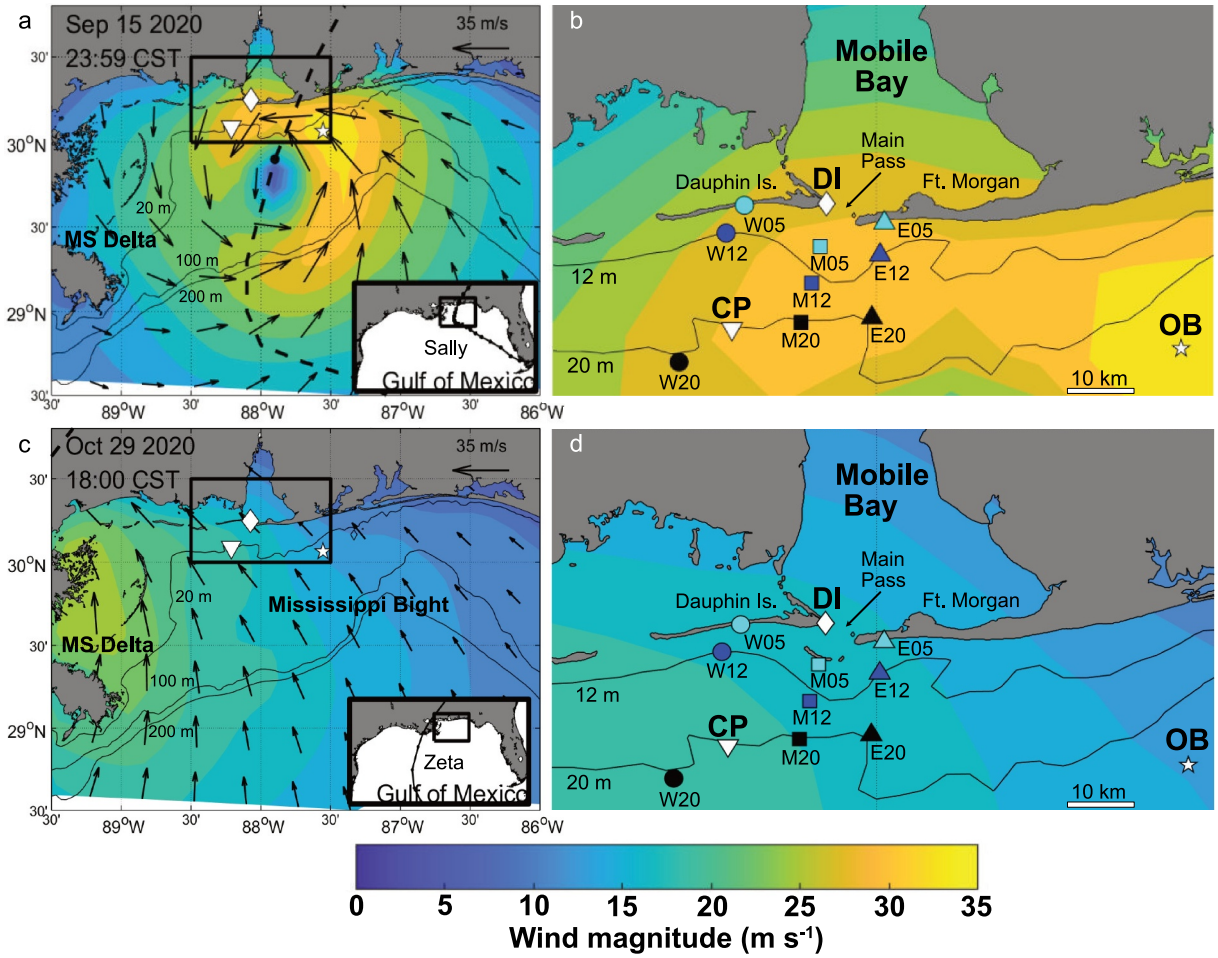

Figure 1. Map of the Mississippi Bight region of the northern Gulf of Mexico displaying (a) Hurricane Sally and (c) Hurricane Zeta wind conditions on 15 September 2020 at 23:59 CST and 29 October 2020 at 18:00 CST, respectively and map of study area and sites during (b) Sally and (d) Zeta bounded by the black boxes in panels (a) and (c). Wind speed is shown in colors, and wind speed and direction (arrows), storm track (dashed line) and location of storm center (black dot) are shown in panels (a) and (c). Hydrological and/or meteorological monitoring stations CP (Coastal Processes; inverted triangle), DI (Dauphin Island; diamond), and OB (Orange Beach; star) are shown by white symbols. Mobile River stations (MR1 and MR2) are north of map boundaries and not depicted. Sampling sites are distinguished by shapes indicating transect (West: circles, Middle: squares, and East: triangles) and colors indicating depth (cyan: 5 m, blue: 12 m, and black: 20 m). Insets in panels (a) and (c) show study area and full storm tracks of Sally and Zeta within the Gulf of Mexico. Thin black lines show selected isobaths. Figure modified and adapted from Dzwonkowski et al., 2022 with permission (©Copyright, 2022 AMS).

1.3. Hurricanes Sally and Zeta

Hurricane Sally crossed the Alabama shelf 15–16 September 2020, rapidly intensifying from a Category 1 to 1 knot short of a Category 3 hurricane with a well-developed eyewall, producing maximum sustained winds of 48.9 m s^{-1}. The storm made landfall near Gulf Shores, AL, around 0345 CST on 16 September 2020 (Figure 1a; Berg & Reinhart, 2021; Dzwonkowski et al., 2022). Six weeks later, Hurricane Zeta made landfall in southeastern Louisiana at around 1600 CST on 28 October 2020, rapidly intensifying from a tropical storm to a Category 3 hurricane just before landfall (Figure 1c; Blake et al., 2021). Over this 6-week time span, the shallow coastal sediments of the Alabama coast faced two of the greatest storm disturbances in over a decade (Figure S2 in Supporting Information S1).

We investigated the short- (10 days) and long-term (6 weeks–8 months) changes to surficial (up to 8–12 cm depth) sediment structure along- and across-shore on the Alabama coast (5–20 m depth) following Hurricanes Sally and Zeta (Figure 1). The depth range was chosen because most known discrete storm sediment beds have been found at 10–20 m depth (i.e., Morton, 1988). We also compared the impacts of Sally and Zeta on sediment structure as they were two major storms with differing physical forcing. Additionally, we compared sediment changes directly

after tropical cyclones to fair-weather changes to assess storm bed preservation potential on a dynamic river-influenced coast. Before and after Hurricanes Sally and Zeta, we collected cores to measure sediment grain size distribution and organic content. We estimated physical forcing on and potential terrestrial sediment inputs to the study area during and outside of the two hurricanes using hydrographic and meteorological monitoring data from several nearby stations as well as hindcast data.

Due to the intense wave action and strong currents flowing to the west-southwest observed during Hurricane Sally (Dzwonkowski et al., 2022; Dzwonkowski & Lockridge, 2021), we hypothesized shallow sediments within the shoreface (5 m; Brutsché et al., 2016; Hollis et al., 2019) would be resuspended and transported by storm currents, leaving behind coarser, sorted sediments with more normal grain size distributions. We expected that deeper sediments (12 and 20 m sites), however, may experience less resuspension but receive sediments transported from shallower areas. This would result in a surficial layer of better sorted and normally distributed sand overlying sediments similar in composition to pre-storm sediments (Keen et al., 2006; Mclaren, 1981). We expected potential storm layers to be thinner or disappear with increasing distance from the storm track (from east to west) and with increasing depth as sand supply and energy declined (e.g., Goff et al., 2010; Hayes, 1967). In absence of sand delivery (e.g., western-most sites), we expected post-storm sediments to experience erosion or winnowing of fine grains, resulting in coarser, better-sorted surface layers.

We also expected differences in storm bed thickness and composition between Sally and Zeta due to differences in physical forcing between the two storms. Because of Zeta's distance from and shorter duration of high winds in the study area compared to Sally (Berg & Reinhart, 2021; Blake et al., 2021), we expected less resuspension and transport and therefore thinner post-Zeta storm beds. Over the months following Sally and Zeta, we expected that there would be an overall increase in mud content at the surface due to a combination of wind-wave resuspension of inshore muds (i.e., in Mobile Bay) and offshore transport driven by predominantly north winds during winter and high riverine inputs during late winter and spring (Dinnel et al., 1990; Stumpf et al., 1993). Alternatively, at sites not receiving transported mud (i.e., away from Mobile Bay plume influence), we expected sediments would either become coarser and better sorted due to continued resuspension during strong winter winds (e.g., 5 m sites) or exhibit little change (12 and 20 m sites). Overall, we expected storm sediment layers would remain mostly intact over the long term due to the extreme nature of hurricanes Sally and Zeta.

2. Materials and Methods

2.1. Core Collection

To determine short and long-term changes to nearshore surficial sediments following hurricanes Sally and Zeta, we collected 1–2 sediment cores (9.6 cm inner diameter; within an approximately 2–3 m radius) per site from 9 sites offshore of Dauphin Island and Fort Morgan, AL along three transects (W: west; M: middle; E: east) at 5 m, 12 m, and 20 m depths 6 days before and 10, 40, 85, 162, and 246 days after Hurricane Sally made landfall (Figure 1). Note that Hurricane Zeta occurred 42 days after Sally. Bottom water salinity and temperature (° C) used for seawater density calculations were also measured at each site and timepoint using a CTD (conductivity, temperature, depth) instrument array. Sites of differing grain sizes (i.e., from mud in the west to sand in the east) were selected based on a previous survey of sediment type (Jenkins, 2011). At the first sampling timepoint, cores were collected at some sites with an Ocean Instruments MC-400 multicorer (sites M05, M12, M20, and W12). Due to difficulties in retrieving cores with the multicorer in sandier sediments, we collected cores via SCUBA diving at the remaining sites and at all subsequent sampling timepoints. Cores were not collected at the 20 m sites in late October due to time and weather constraints. Cores from site E12 before Sally and from site M05 in late May were lost.

2.2. Sediment Characterization

Cores were sectioned into 1-cm increments from 0 to 8–12 cm and oven-dried at 70°C for >48 hr. A subsample was taken from each dried section and combusted at 550°C for 4 hr to remove and quantify organic matter content, then soaked in sodium hexametaphosphate for at least 3 weeks to deflocculate. Grain size distributions were measured using a Malvern Mastersizer 3000 and were compared to visually distinct sediment layers observed in core photographs where available. Grain size metrics (mean grain size, sorting, skewness, and kurtosis) were calculated using GRADISTAT and reported using the Folk and Ward (1957) logarithmic graphical method (Blott & Pye, 2001). See Clemo et al. (2023) for grain size processing details.

2.3. Physical Forcing Estimation

Hydrodynamic forcing on inner shelf sediments during the study period was determined from meteorological and hydrographic data collected at several stations (Figure 1). Wind speed (m s^{-1}) and direction (degrees) and wave characteristics were collected from NOAA National Data Buoy Center (NDBC) stations DPIA1 (eastern Dauphin Island; DI) and 42012 (offshore of Orange beach, 25 m water depth; OB), respectively (Figure 1). Wind data was available from OB, but we used DI wind measurements due to the station's proximity to the study area and its location to the right of the storm track. Along- and across-shelf current speed (m s^{-1}) throughout the water column was measured with a 600 kHz Nortek Acoustic Doppler Waves and Current Profiler (AWAC) at 20 m depth offshore of Dauphin Island at the Dauphin Island Sea Lab Coastal Processes mooring (CP) (Dzwonkowski & Lockridge, 2021; Figure 1). See Dzwonkowski et al. (2021) for current data processing details. To characterize the riverine input to the study area, river gage height (m), and discharge (m^3 s^{-1}) were obtained from US Geological Survey (USGS) Station 02470629 located on the Mobile River (station MR1), 87 km north of the mouth of Mobile Bay near Bucks, AL (31.0157 N, 88.021 W), and historic (1961-present) peak river height (crest; m) was obtained from NOAA Station BCKA1 (station MR2), located approximately 2 km south of MR1 (31.0028 N, 88.0110 W). In addition to wave observations from OB, we obtained significant wave height hindcasts during Sally and Zeta for each sampling site from the Advanced Circulation Model for Oceanic, Coastal and Estuarine Waters (ADCIRC), which were accessed from the Coastal Emergency Risk Assessment (CERA) website (http://cera.coastalrisk.live/). Modeled wave heights during Sally and Zeta obtained at the location of OB were compared to wave height data from OB to assess ADCIRC performance. The modeled wave heights agreed reasonably well with the OB measurements, with slight overestimation during Sally (Figure S3a in Supporting Information S1) and underestimation during Zeta (Figure S3b in Supporting Information S1), when the peak modeled wave height occurring slightly earlier (<2 hr) than peak measured wave height.

Current-generated bed shear stress (τ_{bc}; Pa) at 20 m during Sally was estimated from near-bed current speed measurements at CP using the logarithmic profile method (e.g., Jumars & Nowell, 1984). This method assumes a logarithmic velocity depth profile, so we applied it only to a period of time where the flow of the entire water column at CP appeared to be near steady state (Figures S1c and S1d in Supporting Information S1). Velocity profiles were obtained from 18 measurement points every 0.5 m above the AWAC, from 1.5 m (the closest measurement to the bottom) to 10 m above the bottom at every 0.5 m. Bottom roughness (z_0; m) and shear velocity (u_*; m s^{-1}) were estimated using the Karman-Prandtl equation or "law of the wall" (Boudreau and Jorgensen, 2001; Jumars & Nowell, 1984):

$$u_z = \frac{u_*}{\kappa} \ln\left(\frac{z}{z_0}\right)$$

where u_z is velocity at height z, κ is von Karman's constant (0.41), and z is the height above the seafloor (m). To ensure the validity of the assumption of a logarithmic profile, u_* and z_0 were only determined from ln(z) versus u_z fits with an $R^2 \geq 0.90$. Current-generated bed shear stress (τ_{bc}; Pa) was subsequently calculated from u_* as:

$$\tau_{bc} = {u_*}^2 \rho$$

(e.g., Wheatcroft et al., 2007), where ρ is bottom water density (kg m^{-3}), which was calculated from bottom water salinity and temperature collected at each site (Table 1) and depth (m) using the equation of state for seawater (Jackson & Richardson, 2007). Current shear stress could not be determined at shallower sites due to the lack of current measurements or during Zeta at 20 m because none of the velocity profiles during the storm exhibited a logarithmic fit with an $R^2 \geq 0.90$ (Figures S1e and S1f in Supporting Information S1), indicating none of the measurement depths was within the logarithmic velocity layer.

Near-bed orbital velocity (U_b; m s^{-1}) at each site was estimated from significant wave height (H_s; m) and dominant period (T_{dom}; s) data from OB and CERA hindcast significant wave height data using the parametric method from Wiberg and Sherwood (2008) using Matlab scripts provided in their Appendices D and E. Wave period data were not available from CERA, so we estimated orbital velocity using dominant period from OB and across a range of periods (8–12 s) consistent with the range of dominant periods observed at OB during Sally and

Table 1
Mean Grain Size (μm) of the Top 1 cm, Bottom Water Density (ρ_w; kg m^{-3}) and Estimated Max Significant Wave Height (H_s; m; From CERA) Used for Shear Stress Calculations and Estimated Max Wave-Generated Shear Stress (τ_w; Pa) and Time (h) Shear Stress Was Greater Than or Equal to 1 Pa for Hurricanes Sally and Zeta at Each Site

	Sally					Zeta				
Site	Mean grain size (μm)	ρ_w (kg m^{-3})	Max H_s (m)	Max τ_w (Pa)	Time $\tau_w \geq 1$ Pa (h)	Mean grain size (μm)	ρ_w (kg m^{-3})	Max H_s (m)	Max τ_w (Pa)	Time $\tau_w \geq 1$ Pa (h)
W05	120	1,017	2.34	2.03 (1.82–2.06)	41 (35–42)	80.9	1,021	2.04	1.36 (1.30–1.48)	5 (3–5)
M05	271	1,018	2.91	3.61 (3.34–3.71)	70 (69–72)[b]	270	1,021	3.14	4.09 (3.87–4.25)	20 (19–21)[b]
E05	213	1,017	3.23	4.12 (3.83–4.19)	55 (54–55)	200	1,021	2.56	2.61 (2.43–2.75)	13 (11–15)
W12	18.2	1,018	4.41	1.26 (1.12–1.41)	16 (11–24)	45.0	1,022	4.96	1.94 (1.75–2.18)	5 (4–6)
M12	11.3	1,018	4.89	1.37 (1.20–1.50)	27 (23–31)	271	1,022	5.45	3.80 (3.26–4.04)	9 (8–9)
E12	209[a]	1,017	4.83	2.81 (2.43–3.04)	43 (37–45)	217	1,022	4.73	2.65 (2.38–2.97)	7 (6–7)
W20	159	1,022	5.98	1.87 (1.34–2.06)	27 (19–32)	213[a]	1,021[a]	5.96	1.66 (1.43–2.19)	4 (3–5)
M20	63.4	1,020	6.21	1.60 (1.14–1.75)	22 (12–28)	198[a]	1,021[a]	6.04	1.98 (1.44–2.21)	5 (4–6)
E20	84.2	1,021	6.19	1.70 (1.21–1.87)	24 (14–29)	201[a]	1,021[a]	5.99	1.99 (1.42–2.18)	5 (3–5)

Note. Values used for calculations during Sally and Zeta were taken 6 days before and 40 days after Sally, respectively. Max τ_w and time values and ranges in parentheses are calculated using the corresponding peak wave period from OB and wave periods of 8 and 12 s, respectively. [a]Data not available, values from 10 days post-Sally used instead. [b]Value calculated with 8 s period is greater than value calculated with OB period, so range in parentheses is from OB period to 12 s period.

Zeta. Using equations from Wheatcroft et al. (2007) and Wiberg and Sherwood (2008), wave-generated bed shear stress (τ_{bw}; Pa) was subsequently calculated from near-bed orbital velocity as:

$$\tau_{bw} = 0.5\rho f_w U_b^2$$

Wave friction factor (f_w) was calculated from the near-bed orbital excursion amplitude (a; m) and roughness length (k_s; m):

$$f_w = 0.04(a/k_s)^{-1/4}$$

Mean grain size (m) of the top 1 cm measured at each site 6 days before Sally and 40 days after Sally was used as k_s during Sally and Zeta, respectively (Table 1). Orbital excursion amplitude (a) was calculated as:

$$a = \frac{U_b T_{dom}}{2\pi}$$

Values of roughness length (z_0) determined from current shear stress calculated at CP during Sally (581–1900 μm) were much greater than surface mean grain size (Table 1), and assuming a roughness of mean grain size likely underestimates roughness produced by ripple formation or biological activity (e.g., DuVal et al., 2021). However, due to the lack of current measurements at 5 and 12 m sites, roughness lengths could not be determined from the Karman-Prandtl equation, so grain size was used. Therefore, calculated wave-generated bed shear stresses in this study were likely conservative estimates compared to current-generated shear stress but allowed comparisons of wave-generated shear stresses between sites and depths.

3. Results

3.1. Physical Conditions During Hurricanes Sally and Zeta

Hurricanes Sally and Zeta generated the most intense wind and waves and second-most intense waves, respectively, measured on the Alabama coast since 2009, but the storm impacts differed in their magnitude, duration, and direction (Figures 1 and 2, Figures S1 and S2 in Supporting Information S1). As Sally approached the Alabama coast, winds measured on Dauphin Island exceeded 35 m s^{-1} from the northeast, and the storm drove significant wave heights at NOAA Station 42012 offshore of Orange Beach, AL (Figure 1) exceeding 5 m for over

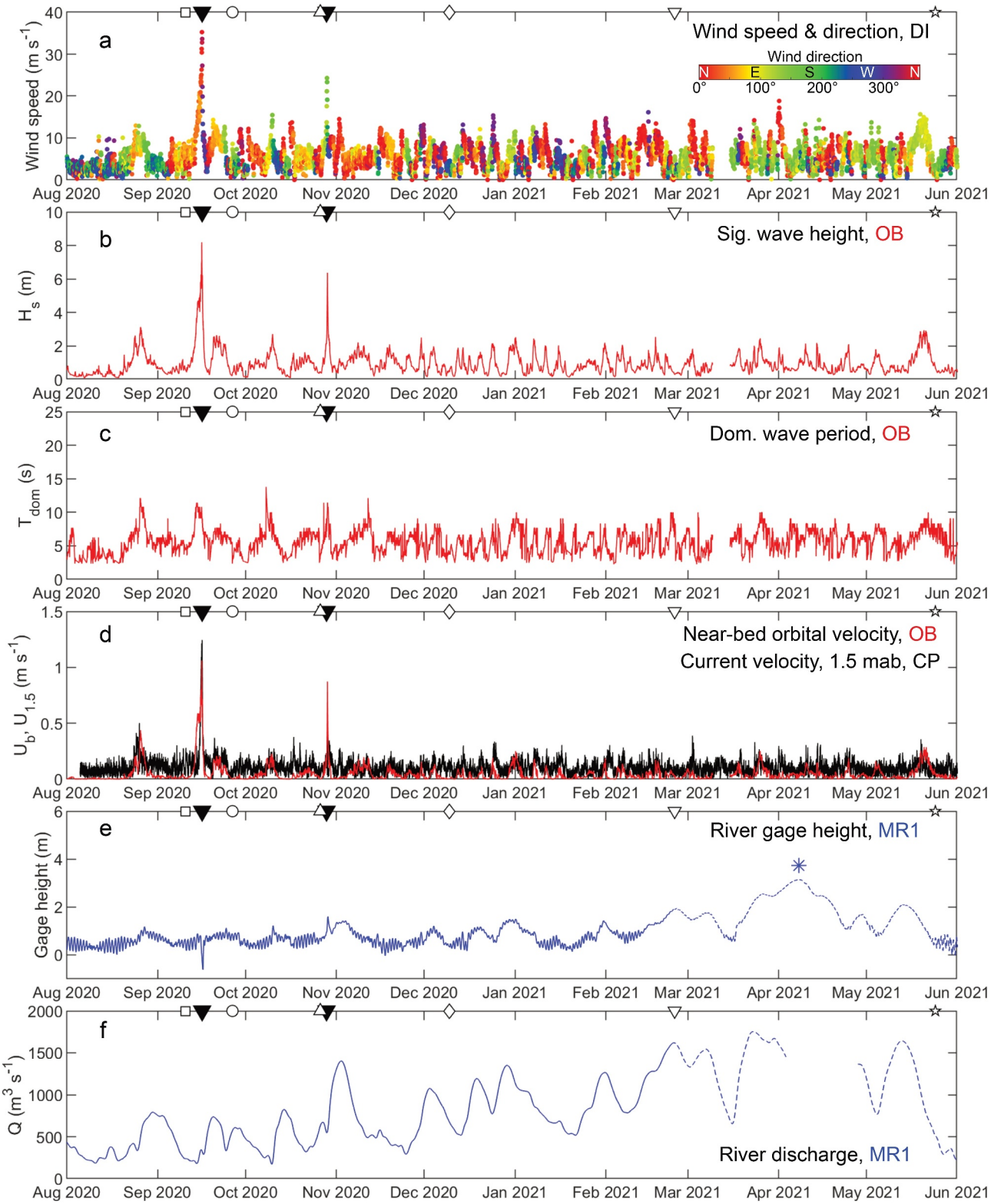

Figure 2.

12 hr, peaking at 8.19 m a few hours after landfall (Figures 2a and 2b). As Hurricane Zeta continued northeastward after landfall in Louisiana, the storm generated winds from the southeast over 24 m s^{-1} and wave heights up to 6.37 m, although waves over 5 m high occurred for a shorter duration than during Sally, approximately 3 hr early on 29 October (Figures 2a–2c). Additionally, Sally's west-southwestward bottom currents, which reached 1.25 m s^{-1} at 20 m depth, far exceeded the southeastward currents produced by Zeta (Figures 1 and 2d, Figure S1 in Supporting Information S1).

Based on wave hindcast model results (CERA), Hurricane Sally generated an intense physical environment at all sites. Estimated wave heights were lowest at the westernmost sites and increased with depth, with estimated peak significant wave height ranging from 2.34 m at W05 to 6.21 m at M20 (Table 1). Wave-generated bed shear stress during Sally, calculated using pre-Sally surface mean grain size as bed roughness (Table 1), generally increased west to east and with decreasing depth, driving maximum shear stresses from around 1 to 2 Pa at 20 m to 2–4 Pa at 5 m (Table 1, Figures 3a, 3c and 3e). Compared to the other sites, E12 shear stress may have been overestimated because pre-Sally mean grain size was not available at this site so post-Sally grain size was used for bottom roughness (Table 1). Additionally, bottom currents measured at 1.5 m above bottom at CP at 20 m reached 1.25 m s^{-1}, driving estimated current shear stresses up to 6.3 Pa (Figure 3e). Thus, combined wave and current shear stresses at all sites were likely much greater than wave-generated shear stress alone.

Six weeks later, Hurricane Zeta passed to the west of the study area (Figure 1c) and generated similar wave heights to Hurricane Sally but for a much shorter duration. At 5 m depth, Zeta's waves generated shear stresses capable of transporting coarse sand (i.e., >1 Pa; Nowell et al., 1981) for periods ranging from a few hours at W05 to just under a day at M05 (Table 1, Figure 3b). Similarly, although peak shear stress during Zeta was greater than during Sally at some 12 and 20 m sites, it only exceeded 1 Pa for <10 hr (Table 1, Figures 3d and 3f). In addition, whereas Hurricane Sally generated >1 m s^{-1} currents for 8 hr during an extended period of high waves at 20 m depth, bottom currents during Zeta were <0.4 m s^{-1} (Figure 2d, Figure S1 in Supporting Information S1). In contrast to the drop in river gage height and relatively low river discharge during and after Sally, Zeta caused a notable peak in river gage height and post-storm river discharge (Figures 2e and 2f).

3.2. Pre-Sally Spatial Variability of Sediment Structure

Prior to Hurricane Sally, Alabama coastal sediments exhibited high spatial variability. The surficial sediments at W05, the westernmost 5 m site, were muddier and more heterogenous with depth (54–373 μm) compared to the more homogenous clean sands at the middle and eastern 5 m sites, M05 (253–279 μm) and E05 (208–237 μm) (Figures 4a, 4c, and 4e, Figure S4 in Supporting Information S1). W05 sediments were generally poorly sorted and finely skewed medium to fine sand with 10%–15% mud content, exhibiting some sharp transitions from sand to mud (e.g., 373 μm at 5 cm vs. 54 μm at 6 cm) (Figure 4a, Figures S4a–S4g in Supporting Information S1). We also visually observed darker-colored mud underlying the surficial muddy sand in some cores used for other measurements that were not sectioned for grain size (Figure S5a in Supporting Information S1).

Sediments at 12 m did not exhibit an along-shelf gradient and were generally muddier than 5 m sites (Figures 4g and 4i, Figure S6 in Supporting Information S1). W12 and M12 sediments consisted of medium to fine silts (11–26 μm) that were mostly poorly to very poorly sorted, normal to fine-skewed, with no distinct layers (Figures 4g, 4i and 5b, and 5f, Figures S6a–S6n in Supporting Information S1). The cores from E12 were not sectioned, but one core displayed 4–5 cm of lighter-colored sandy mud or muddy sand overlying darker mud (Figure S5b in Supporting Information S1).

Sediments at 20 m were coarser than at 12 m, mostly finer than 5 m sediments, and lacked the expected along-shelf gradient (Figures 3l, 3n, and 3p, Figure S7 in Supporting Information S1). W20 sediment was relatively homogenous with depth, consisting of mostly moderately well sorted fine sand (157–216 μm) with a normal distribution, and had a slightly muddier surface layer (0–2 cm: 11%–12% mud; 3–10 cm: 2%–5% mud; Figures 3l,

Figure 2. Time series of (a) wind speed and direction at station DI, (b) significant wave height (H_s), (c) dominant period (T_{dom}), and (d) estimated near-bed orbital velocity (U_b) at station OB (red) and current speed at 1.5 m above the seafloor ($U_{1.5}$) at station CP (black), (e) river gage (blue line) and historic crest height (blue asterisk; Station MR2) and (f) discharge (Q) on the Mobile River at station MR1 from 1 August 2020–1 June 2021. White symbols indicate sampling dates and black triangles mark landfall dates of hurricanes Sally and Zeta. Dashed lines in panels (e) and (f) indicate provisional data. Note that for panels (a), (d), wind direction is the direction from which the wind is blowing versus current direction is the direction to which the current is flowing.

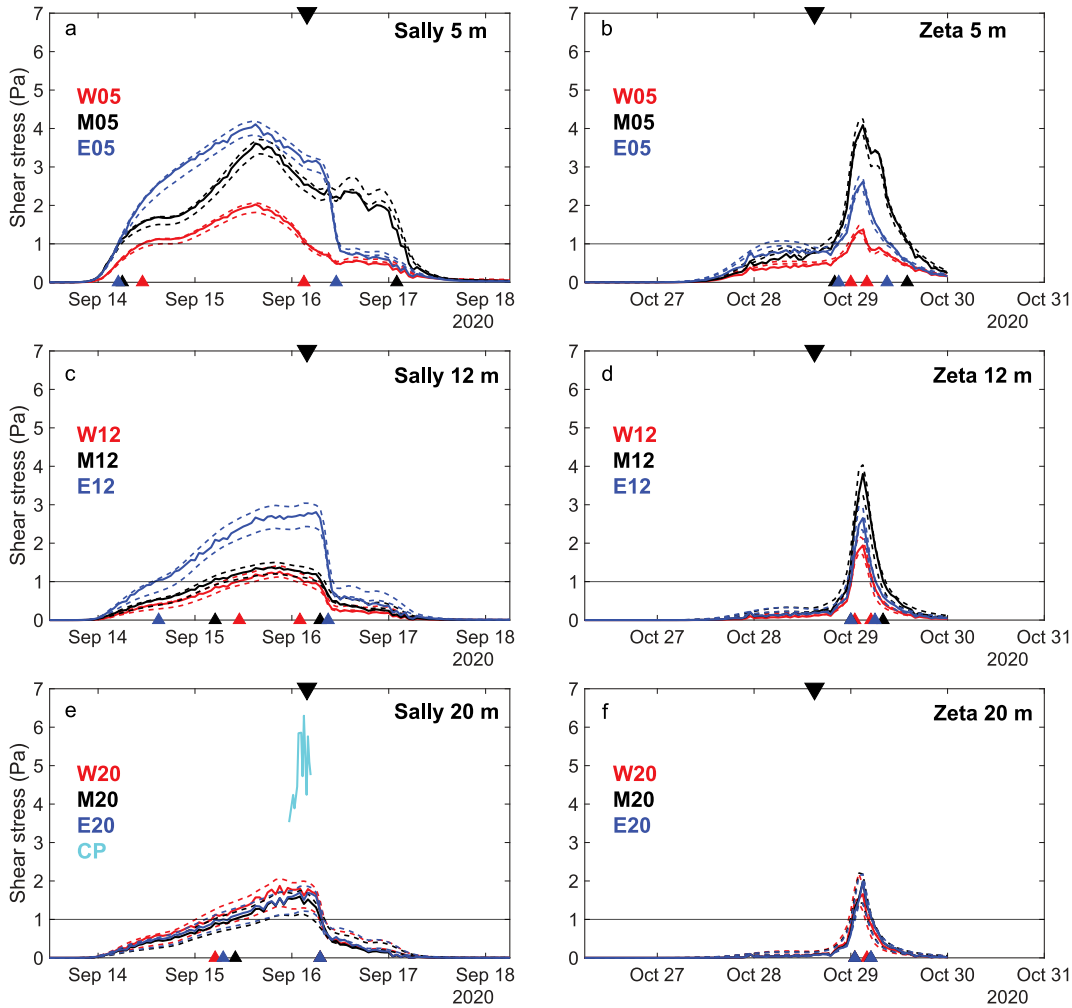

Figure 3. Wave-generated bed shear stress estimated from CERA hindcast data at (a–b) 5 m, (c–d) 12 m, and (e–f) 20 m sites during hurricanes Sally and Zeta and (e) current-generated bed shear stress at site CP (20 m depth). Shear stresses estimated from hindcast wave height data are shown for observed time-varying wave periods from OB (solid line) and wave periods of 8 and 12 s (low and high dashed lines, respectively). West, middle and east transects are shown in red, black, and blue, respectively. Current shear stress estimated from current data at CP is indicated by the cyan solid line (e). Large black triangles mark landfall dates of Sally and Zeta, and small red, black, and blue triangles mark intervals where shear stress was ≥1 Pa (horizontal line) for west, middle, and east transects, respectively.

5a, and 5v Figures S7a–S7g in Supporting Information S1). E20 exhibited a 2 cm thick layer of fine sand at 4–5 cm similar to W20 (178–190 μm) that was bracketed above and below by muddier (18%–25% mud), poorly sorted, and very fine skewed very fine sand (84–167 μm) (Figures 4p and 5d, Figures S7o–S7u in Supporting Information S1). At M20, the sediment was muddier and more poorly sorted than the other 20 m sites (34–78 μm, 25%–58% mud) (Figures 4n and 5c, Figures S7h–S7n in Supporting Information S1).

3.3. Post-Sally Spatial Variability of Sediment Structure

Changes in surficial sediments on the Alabama shelf following Hurricane Sally varied substantially across the 9 sites. Despite over 2 days of shear stresses exceeding 1 Pa (Figure 3a), the sandy 5 m sites appeared to change little, with M05 and E05 remaining moderately well-sorted clean sands (194–270 μm) 10 days after Sally (Figures 4d–4f, Figures S4h–S4u in Supporting Information S1). Post-Sally sediment at W05 was mostly muddier and less variable with depth, although the duplicate cores exhibited substantially different grain size compositions (19–61 μm and 37%–78% mud vs. 78–129 μm and 14%–25% mud) (Figure 4b, Figures S4a–S4g in Supporting Information S1). Silts at W12 did not exhibit distinct sedimentary structures, consistent with our expectation of

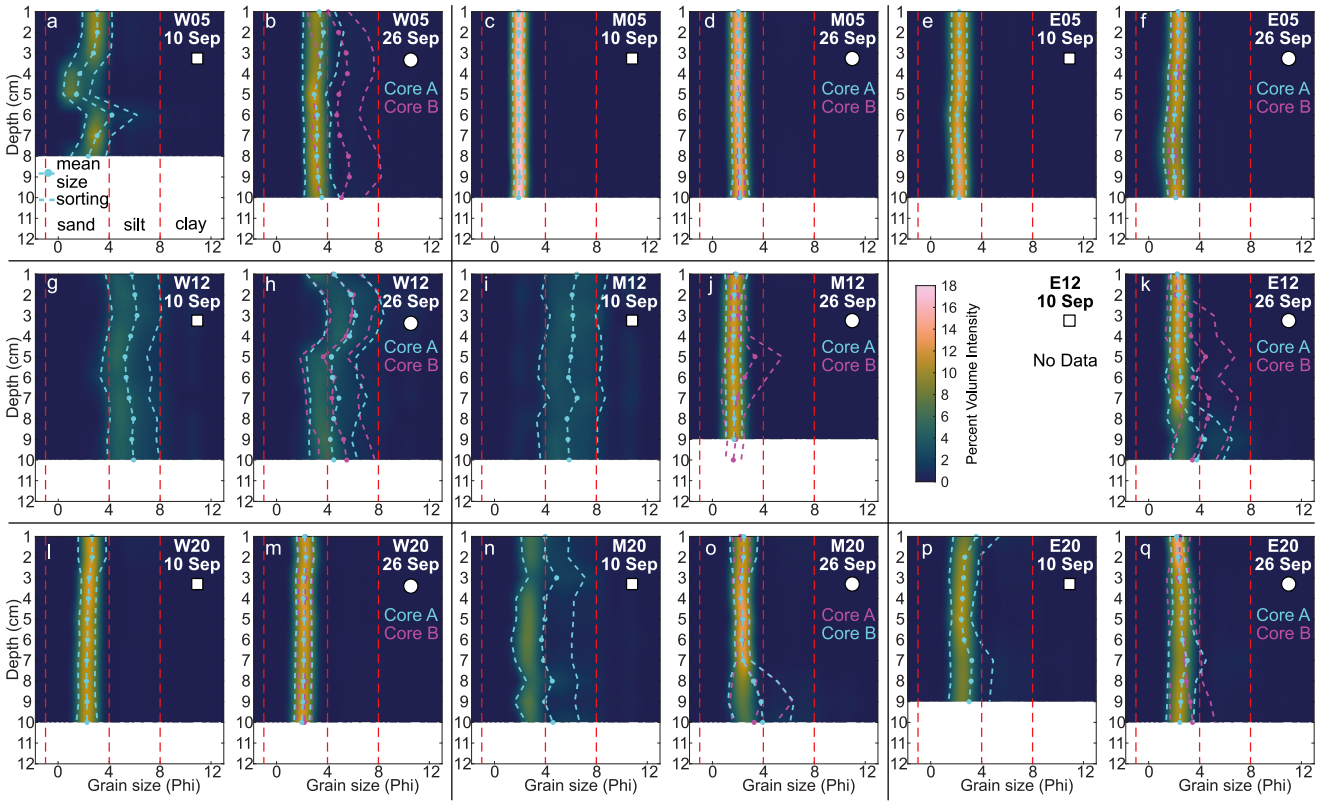

Figure 4. Profiles of grain size distribution (color gradient), mean grain size (φ; colored circles) and standard deviation (i.e., sorting; colored dashed lines) before (10 September 2020) and after Hurricane Sally (26 September 2020) at (a–f) 5 m, (g–k) 12 m, and (l–q) 20 m sites. Pre-Sally data from site E12 are unavailable. Grain size and sorting of replicate cores for which the color gradient is plotted are shown in cyan while other core is shown in magenta. "A" and "B" indicate replicate cores for post-Sally sampling. Color intensity reflects the percent volume of each grain size class for each layer. Vertical red dashed lines indicate sand, silt, and clay size class boundaries. Squares and circles indicate pre- and post-Sally sampling time points, respectively, and correspond to sampling time points in Figure 2.

storm-transported sand thinning further away from the storm center. However, after experiencing a long period of high shear stress (>1 Pa for 10–24 hr; Figure 3c), W12 sediments coarsened some but did not become better sorted or less finely skewed as would be expected with fine sediment winnowing (13–79 μm) (Figure 4h, Figures S6a–S6g in Supporting Information S1). Sediments at E12 displayed moderately well sorted and normally distributed sand (100–231 μm) overlying poorly sorted and very fine skewed mud (38–92 μm) after Sally, but pre-Sally cores also appeared to exhibit similar layering, suggesting few pre- and post-Sally differences at this site (Figure 4k, Figures S5b, S6o–S6u in Supporting Information S1).

Sediments at site M12 and the 20 m sites exhibited changes that were more consistent with expected tropical cyclone impacts. Following 23–31 hr of estimated wave-generated bed shear stresses exceeding 1 Pa during Sally (Figure 3c), M12 sediments shifted dramatically from silts with little sand (11–19 μm, >77% mud) to mainly clean (most layers <10% mud), better-sorted, and more normally distributed medium sands (98–334 μm) 10 days after Sally, consistent with substantial deposition of >10 cm of sand during Sally (Figures 3b, 3f, and 4j, Figures S6h–S6n in Supporting Information S1). In the second core, there was a muddier layer present at 5–6 cm (98–173 μm), but this layer was still much coarser than any pre-Sally layer at M12 (Figure 4j, Figure S6i in Supporting Information S1). Similarly, at M20, 10 days after 12–28 hr of >1 Pa of wave-generated shear stress and up to 6.3 Pa current shear stress (Figure 3e), cores exhibited a 7-cm layer of mostly moderately well sorted and normally distributed fine sand (180–222 μm) overlying muddy sand similar in composition to the pre-Sally sediment (65–108 μm) (Figures 4o and 5c, Figures S7h–7n in Supporting Information S1).

Unexpectedly, neither the westernmost nor easternmost 20 m sites exhibited the post-Sally sand layers observed at M12 and M20 despite W20 and E20 experiencing equivalent to slightly higher shear stresses relative to M20 during Hurricane Sally (Figure 3e). At W20, the post-Sally fine sands remained similar to pre-Sally sediment (201–255 μm) but lacked the finer, more poorly sorted, and finer skewed 2 cm thick surface layer observed before

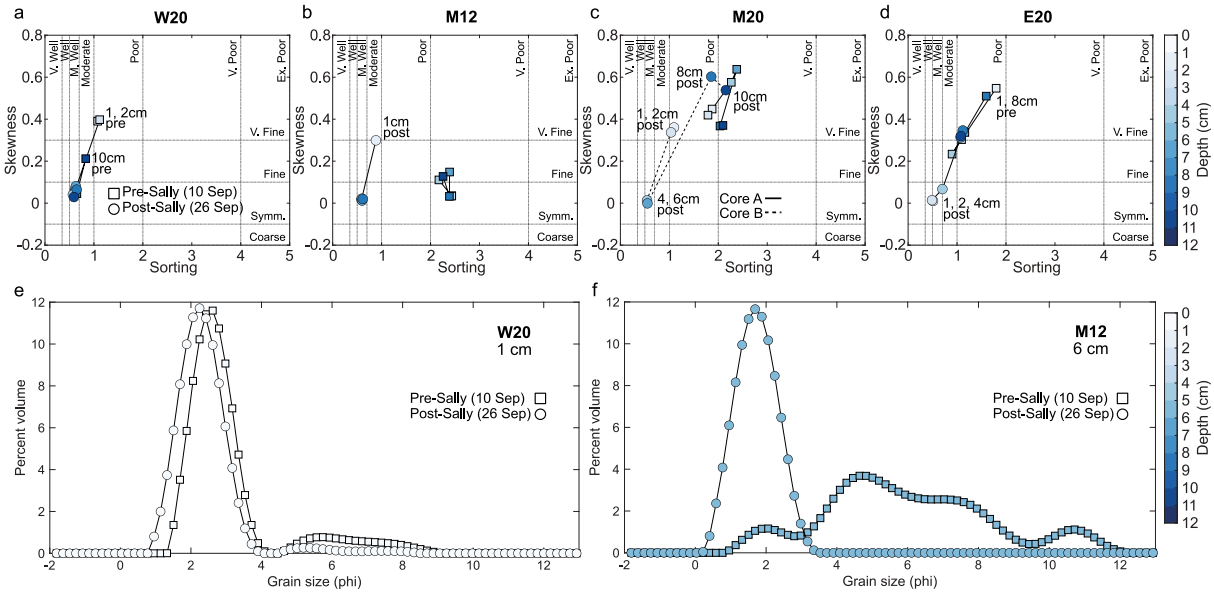

Figure 5. (a–d) Relationship of skewness and sorting before and after Sally for selected sites exhibiting grain size changes consistent with hurricane impacts. Symbol colors correspond to sediment depth (only 1, 2, 4, 6, 8, and 10 cm depths shown) and connecting lines indicate replicates (solid for core A and dashed for core B; only one replicate shown). Examples of grain size distributions shifting from more poorly sorted and finer skewed before Sally to better sorted and more symmetrically distributed after Sally at (e) W20 (1 cm depth) and (f) M12 (6 cm depth). Symbol colors and connecting lines are the same as in panels (a–d). Squares and circles indicate pre- and post-Sally sampling time points, respectively, and correspond to sampling time points in Figure 2.

Sally (Figures 3a, 3e, and 4m, Figures S7a–S7g in Supporting Information S1). Similarly, the top 3–4 cm of sediment at E20 became better sorted and more normally distributed while the underlying sediment composition changed little (91–219 μm) (Figures 3d and 4q, Figures S7o–S7u in Supporting Information S1).

3.4. Pre-Zeta Spatial Variability of Sediment Structure

In late October, just before Hurricane Zeta made landfall, the sediment at 5 m sites was mostly similar to the sediment 10 days after Hurricane Sally, remaining muddy sand at W05 (47–161 μm) and clean sands at M05 and E05 (135–294 μm) (Figure 6a, Figure S4 in Supporting Information S1). There was, however, some coarsening at M05 between post-Sally and pre-Zeta (Figure S4h in Supporting Information S1). W12 remained muddy but generally coarser than pre-Sally and exhibited some coarser and finer layering (16–66 μm), whereas sediment at E12 exhibited similar layering to post-Sally, with 5–6 cm of mostly clean sand (190–260 μm, 0%–6% mud) overlying muddier sediment (25–97 μm, 24%–71% mud) (Figure 6e, Figures S6a–S6g, S6o–S6u in Supporting Information S1). At M12, before Zeta, a mud layer similar in composition to pre-Sally M12 medium to fine silts (8–54 μm) appeared beneath 3–6 cm of clean sand (139–292 μm) similar to that observed 10 days after Sally, suggesting the base of the potential sandy storm layer was not captured by cores taken 10 days after Sally (Figures 7a and 7c).

3.5. Short-Term Post-Zeta Spatial Variability of Sediment Structure

Following Zeta, the sediment at W05 became much coarser and cleaner (62–203 μm) and the clean sands at M05 and E05 (216–274 μm) became slightly better sorted compared to the pre-Zeta sediment (Figure 6b, Figure S4 in Supporting Information S1). Additionally, E05 became somewhat coarser (252–274 μm) (Figure S4o in Supporting Information S1). The coarse to medium silts at W12 did not change appreciably between pre-Zeta and six weeks after (16–62 μm) (Figures S6a–S6g in Supporting Information S1). The surface sandier layer observed at E12 after Sally also appeared to change little in thickness after Zeta (Figure 6f, Figures S6o–S6u in Supporting Information S1). However, the top 1 cm at E12 became slightly muddier, more poorly sorted and more finely skewed (162–211 μm) (Figure 6f, Figures S6o–S6u in Supporting Information S1). M12 sediments remained composed of sand (222–274 μm) overlying mud (9–64 μm), but the sand layer hypothesized to be deposited by Hurricane Sally appeared to have thinned somewhat (3–6 cm to 2–3 cm) after high shear stresses during Zeta

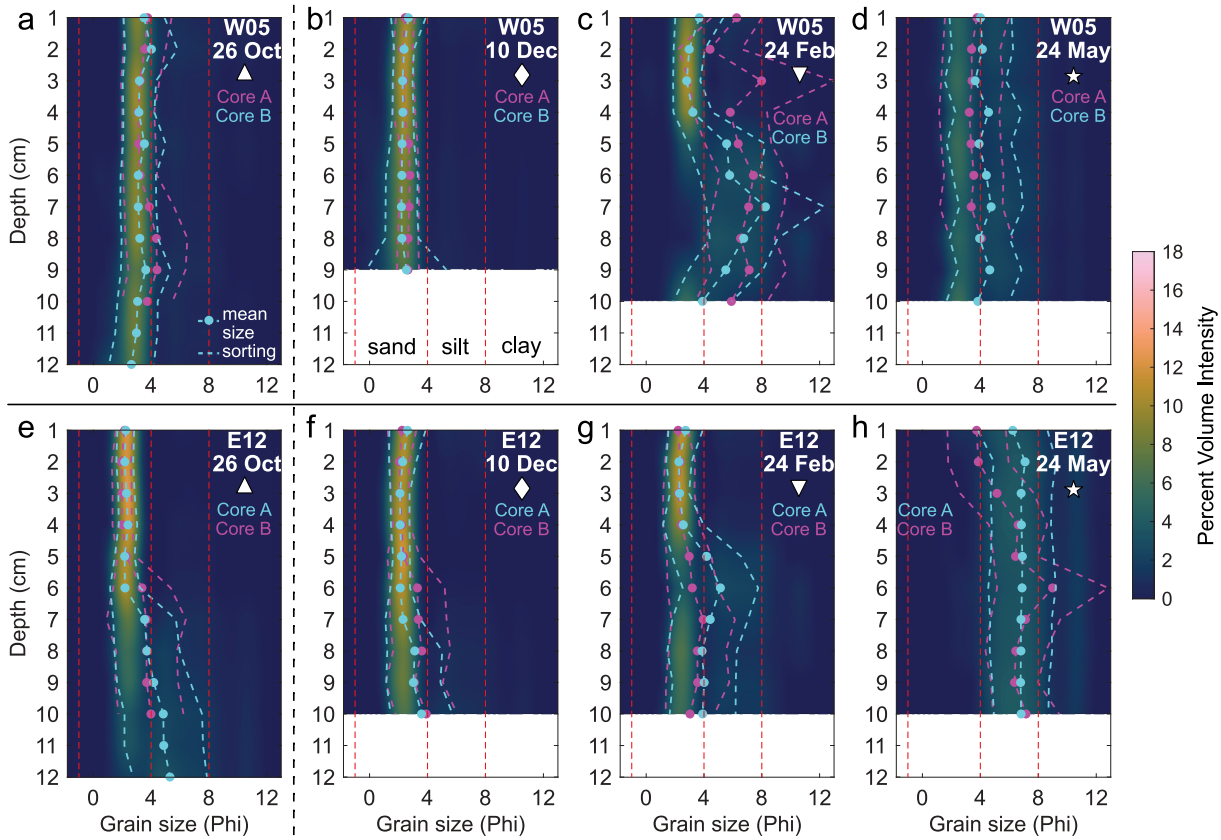

Figure 6. Profiles of grain size distribution (color gradient), mean grain size (φ; colored circles) and sorting (colored dashed lines) from (a, e) before Hurricane Zeta to (d, h) late May at sites (a–d) W05 and (e–h) E12. Grain size and sorting of replicate cores for which the color gradient is plotted are shown in cyan while other core is shown in magenta. "A" and "B" indicate replicate cores. Color intensity reflects the percent volume of each grain size class for each layer. Vertical black dashed line between profiles from 26 October and 10 December indicates Hurricane Zeta. Vertical red dashed lines indicate sand, silt, and clay size class boundaries. Shapes correspond to sampling time points in Figure 2.

(Figures 3d, 7b, and 7c). Cores from M12 also exhibited some variability, with the first core generally coarser than the second core (Figure 7b, Figures S6h–S6n in Supporting Information S1).

Similar to M12 layering, the post-Sally fine sand layer at M20 seemed to change little, appearing somewhat thicker than the post-Sally layer (9 to ≥10 cm) but remaining composed of mostly moderately well-sorted and normally distributed fine sand after Zeta (94–231 μm) (Figures 7e and 7f, Figures S7h–S7n in Supporting Information S1; 20 m sites were not sampled in October due to logistical constraints). Sediments at W20 six weeks after Zeta were somewhat coarser than 10 days after Sally (253–315 μm), but remained mostly homogenous with depth (Figures 8b and 8c, Figures S7a–S7g in Supporting Information S1). At E20, the better sorted and more normal fine sand layer (166–193 μm) overlying poorly sorted and very fine skewed fine to very fine sand (98–163 μm) also remained relatively unchanged compared to following Sally, apart from a slightly more poorly sorted and more finely skewed surface layer (Figures 8e, 8f, Figures S7o–S7u in Supporting Information S1).

3.6. Long-Term Post-Zeta Spatial Variability of Sediment Structure Over Winter and Spring

Between December and late February, the Alabama coast experienced frequent periods of strong winds from the north and northwest (>15 m s^{-1}) and elevated, but not unseasonably high, river discharge (Figures 2a and 2f, Figures S2e and S2f in Supporting Information S1). The sediment at W05 became muddier (3–143 μm and up to 93% mud), more poorly sorted, mostly finer skewed, and more variable with depth, but also heterogeneous, with the second core exhibiting a 4 cm sandy surface layer (78–143 μm) on top of mud (3–67 μm) (Figure 6c, Figures S4a–S4g in Supporting Information S1). In contrast, M05 and E05 sands (205–272 μm) and W12 silts (20–60 μm) appeared to change little over the winter (Figures S4h–S4u and S6a–S6g in Supporting Information S1).

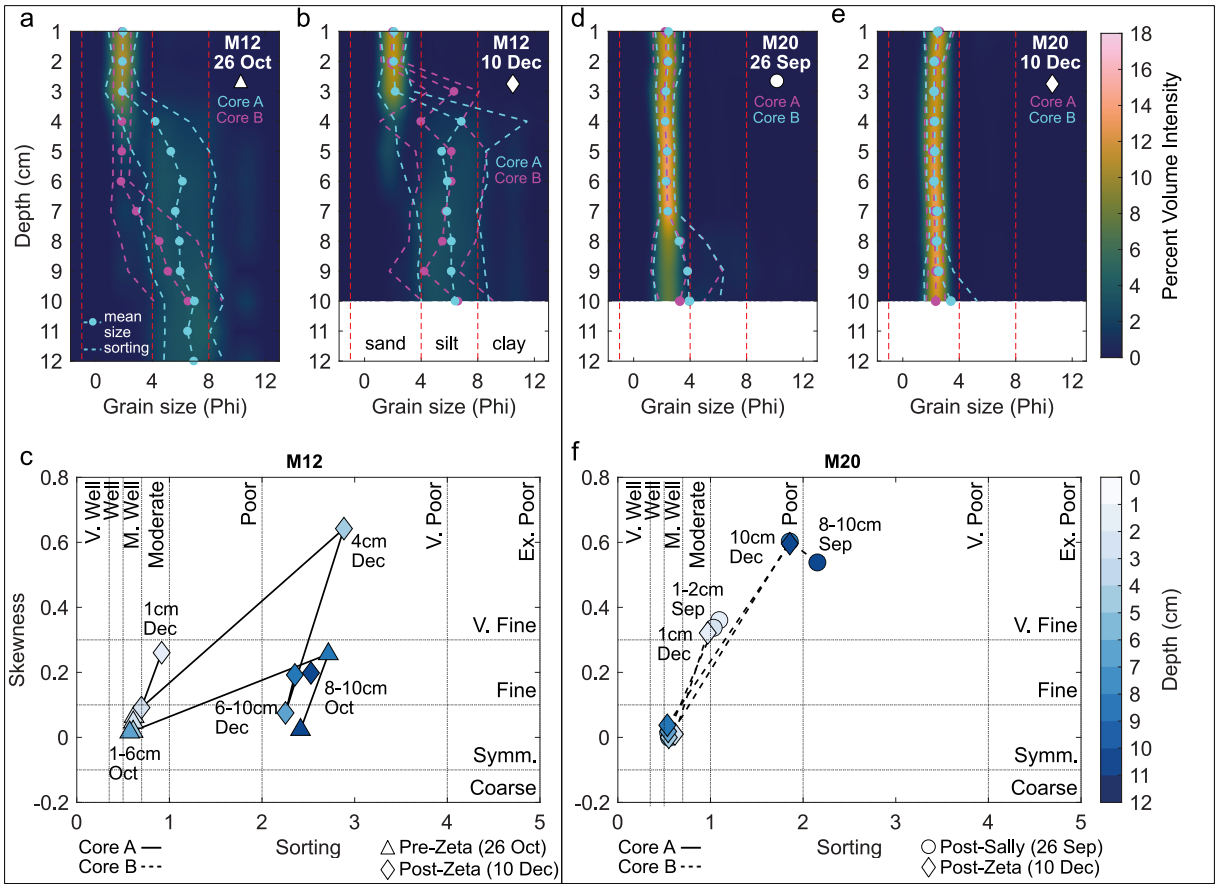

Figure 7. Profiles of grain size distribution (color gradient), mean grain size (φ; colored circles) and sorting (colored dashed lines) before and after Hurricane Zeta at sites showing appearance of distinct sand layers after Hurricane Sally (a–b: M12 and d–e: M20). Sediment was not collected in late October at 20 m sites. Grain size and sorting of replicate cores for which the color gradient is plotted are shown in cyan while other core is shown in magenta. "A" and "B" indicate replicate cores. Color intensity reflects the percent volume of each grain size class for each layer. Vertical red dashed lines indicate sand, silt, and clay size class boundaries. Relationship of skewness and sorting before and after Zeta for sites (c) M12 and (f) M20. Symbol colors correspond to sediment depth (only 1, 2, 4, 6, 8, and 10 cm depths shown) and connecting lines indicate replicates (solid for core A and dashed for core B; only one replicate shown). Shapes correspond to sampling time points in Figure 2.

The sand layers at M12 and E12 appeared to change in thickness after the storms. At M12, the mostly clean fine sand layer (158–313 μm) increased in thickness (6–7 cm) between December and late February but varied between cores (Figure 9b, Figures S6h–S6n in Supporting Information S1). In contrast, the fine sand layer at E12 (127–216 μm) appeared to thin slightly from 5 to 7 cm in December to 4 cm in late February (Figure 6g, Figures S6o–S6u in Supporting Information S1). Further offshore, the strong winter winds generated several periods of >2 m waves at OB and >0.3 m s^{-1} currents at CP (Figures 2a, 2b, and 2d, Figures S1a and S1b in Supporting Information S1), and the two cores from M20 exhibited contrasting layering changes. Most of the first core was composed of fine sand similar to post-Sally and post-Zeta sandy layers (189–231 μm) below a muddier (92–163 μm, 13%–28% mud) 3-cm thick surface layer. The second core was comprised of fine sand (128–220 μm) over very fine sand (82–110 μm) that was similar to the layering observed at M20 after Sally and Zeta (Figures 9f and 9h, Figures S7h–S7n in Supporting Information S1). The sediment at W20, however, became slightly finer over the winter and more similar to post-Sally (196–269 μm), but remained moderately well sorted and normally distributed, and E20 sediment composition also changed little, exhibiting a 5 cm layer of better sorted and more normally distributed fine sand (170–196 μm) above fine to very fine sand (105–168 μm) (Figures 10b, 10d, 10f, and 10h, Figures S7a–S7g, S7o–S7u in Supporting Information S1).

Over the spring, strong winds continued to impact the study area, including winds from the north reaching 18.8 m s^{-1} on 1 April 2021 and an unseasonable 5-day period of winds from the southeast >10 m s^{-1} in mid-May 2021 (Figure 2a, Figure S2a in Supporting Information S1). Additionally, riverine inputs to the coast were high, with peak discharge at MR1 occurring in March and April, including the 23rd highest river crest since 1961 at MR2

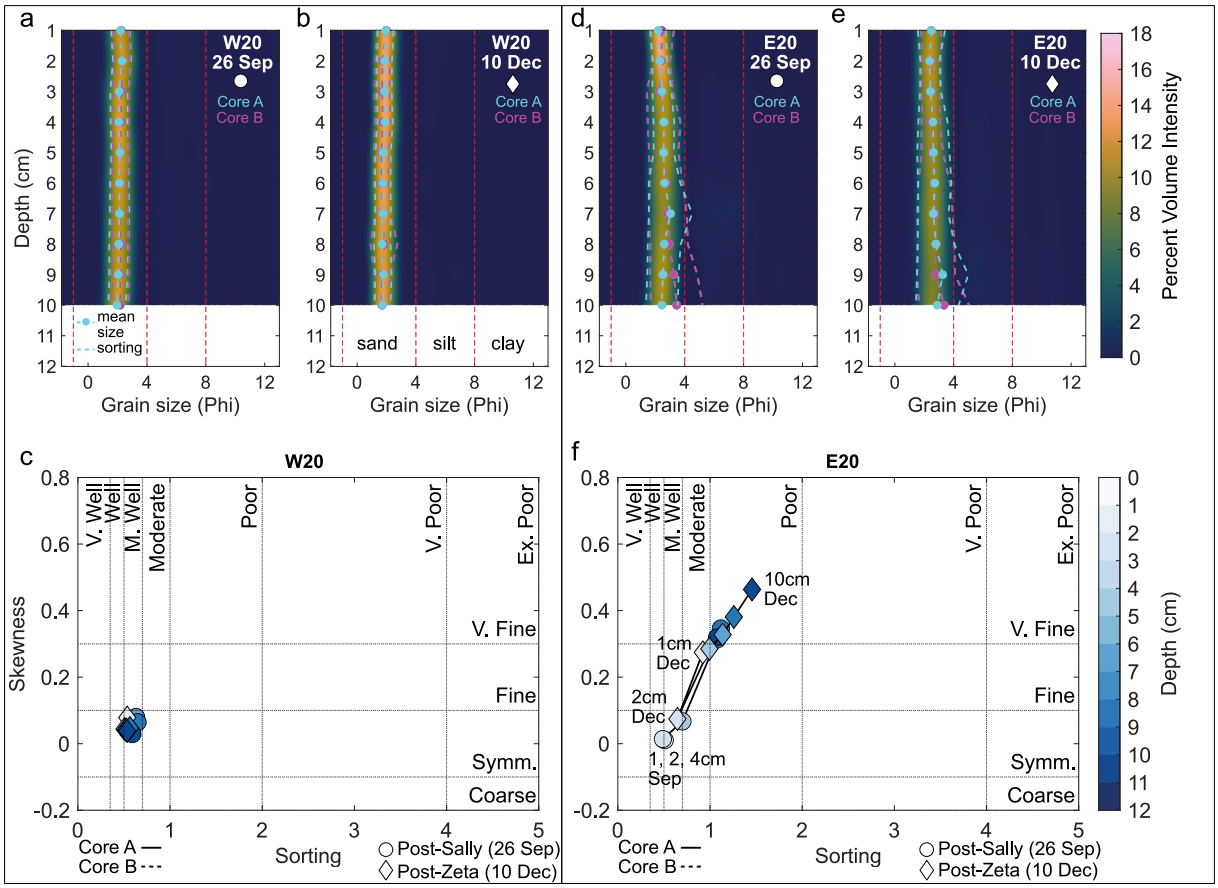

Figure 8. Profiles of grain size distribution (color gradient), mean grain size (φ; colored circles) and sorting (colored dashed lines) before and after Hurricane Zeta at sites that had experienced near-surface grain size changes consistent with winnowing of finer grains during Sally (a–c: W20 and d–f: E20). Sediment was not collected in late October at 20 m sites. "A" and "B" indicate replicate cores. Grain size and sorting of replicate cores for which the color gradient is plotted are shown in cyan and the other core is shown in magenta. Color intensity reflects the percent volume of each grain size class for each layer. Vertical red dashed lines indicate sand, silt, and clay size class boundaries. Relationship of skewness and sorting for sites (c) W20 and (f) E20. Symbol colors correspond to sediment depth (only 1, 2, 4, 6, 8, and 10 cm depths shown) and connecting lines indicate replicates (solid for core A; only one replicate shown). Shapes correspond to sampling time points in Figure 2.

(NOAA Station BCKA1) (Figures 2e and 2f). By late May, following these high winds and flooding, changes to sediment structure were highly variable. Sediments at W05 became sandier (37–106 μm) but remained poorly sorted and muddier than before Hurricane Sally and became more finely skewed (Figure 6d, Figures S4a–S4g in Supporting Information S1). W05 sediments were also similar in appearance to the pre-Sally mud layer visually observed beneath the muddy sand layer sampled (Figure S5a in Supporting Information S1). Sampling equipment was lost at M05 and cores were not collected at this site, but E05 sediment characteristics changed little, apart from some slight coarsening of the top 6 cm (240–280 μm) (Figures S4o–S4u in Supporting Information S1). W12 sediments were somewhat muddier than in late February, but overall sediment composition changed little (16–94 μm) (Figures S6a–S6g in Supporting Information S1). Sediment at E12, on the other hand, changed dramatically, shifting from sand overlying muddy sand that was likely present prior to Hurricane Sally (Figure S5b in Supporting Information S1) to fine silt to clay (2–75 μm) (Figure 6h, Figures S6o–S6u in Supporting Information S1). Most of the sediment at this site contained much more organic-rich mud (64.4%–97.3% mud and up to 17.9% organic content) than any previous timepoint at this site (Figures S6p and S6u in Supporting Information S1). This fine layer was observed to extend at least 30 cm deep in longer cores collected for other measurements.

At M12, the sand-over-mud layering captured in cores from pre-Zeta to late February was observed in some unsectioned cores in late May, but the sand layer appeared to increase in thickness such that the grain size cores did not capture the mud layer (Figure 9c). The sand layer, however, appeared to have slightly coarsened and become slightly better sorted and more normally distributed by late May (260–320 μm) (Figures 9c and 9d, Figures S6h–S6n in Supporting Information S1). At 20 m, there were several instances of strong currents at CP

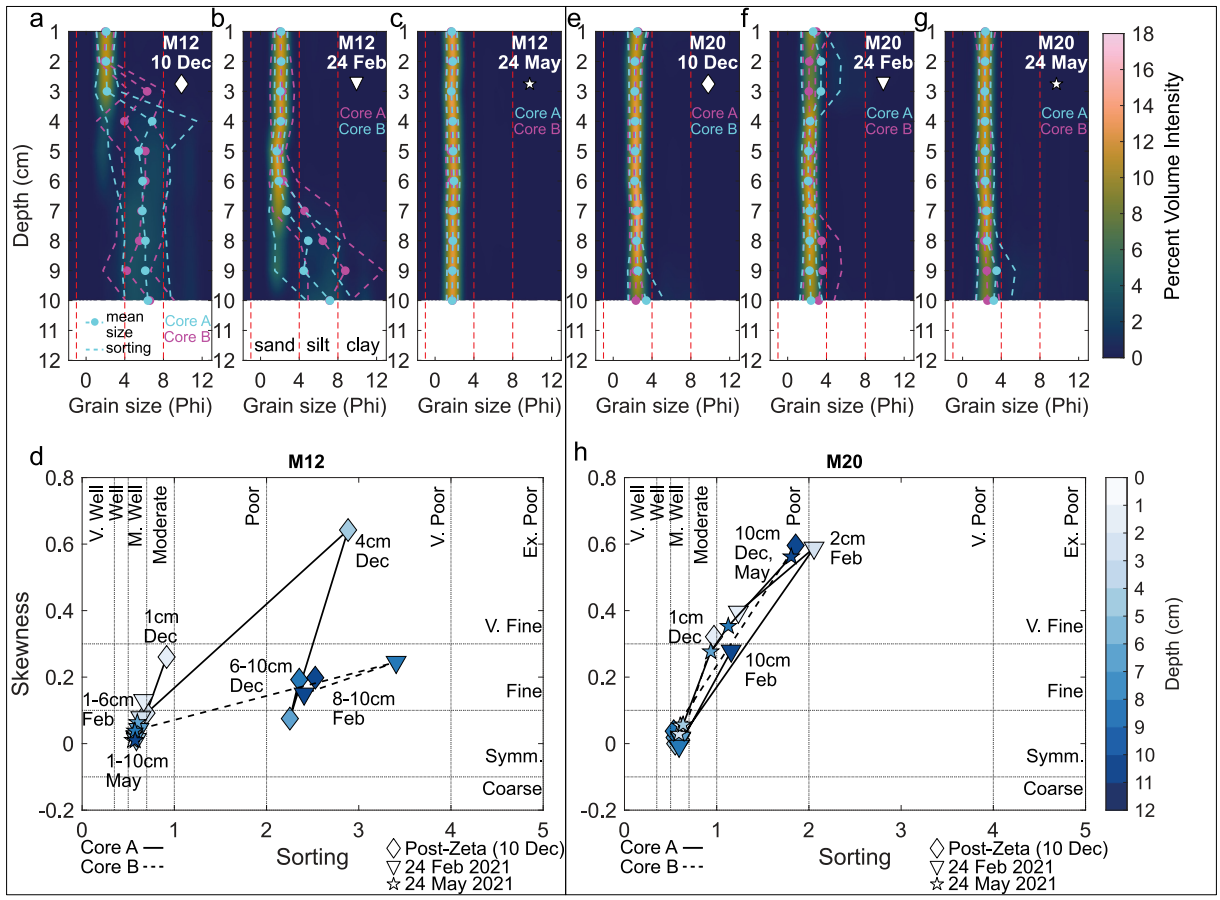

Figure 9. Profiles of grain size distribution (color gradient), mean grain size (φ; colored circles) and sorting (colored dashed lines) from (a), (e) after Hurricane Zeta to (b), (f) late February and (c), (g) late May at sites showing appearance of distinct surface sand layers after Sally (a–d: M12 and e–h: M20). Grain size and sorting of replicate cores for which the color gradient is plotted are shown in cyan while other core is shown in magenta. "A" and "B" indicate replicate cores for a given site and time point. Color intensity reflects the percent volume of each grain size class for each layer. Vertical red dashed lines indicate sand, silt, and clay size class boundaries. Relationship of skewness and sorting for sites (d) M12 and (h) M20. Symbol colors correspond to sediment depth (only 1, 2, 4, 6, 8, and 10 cm depths shown) and connecting lines indicate replicates (solid for core A and dashed for core B; only one replicate shown). Shapes correspond to sampling time points in Figure 2.

over the spring, and by late May, shortly after several days of >2 m waves at OB and up to 0.37 m s^{-1} currents (Figures 2b and 2d, Figures S1a and S1b in Supporting Information S1), the muddier surface layer observed at M20 in one core in late February was absent and the sediment exhibited the better sorted and more normal sand layer (168–214 μm) over muddier, more poorly sorted, and finer skewed sediment layering (88–107 μm) observed at this site since Hurricane Sally (Figures 4o, 5c, 9g, and 9h, Figures S7h–S7n in Supporting Information S1). The sand layer thickness at M20 was similar between December and late May (7 to ≥10 cm) despite record-setting river height at MR2 in April (Figures 2e, 9e, 9g, and 9h, Figure S2e in Supporting Information S1). W20 sediment also returned to a composition similar to the sediment at this site in December (295–354 μm) and sediments at E20 retained the better sorted and more normally distributed surface layer (3–6 cm) of fine sand (156–198 μm) overlying muddier sand (100–162 μm) observed in December and late February (Figure 10). In contrast to the sedimentary fluctuations at W05 and drastic mud increase at E12 (Figure 6), and despite strong winds, waves and currents and high riverine inputs to the coast during the spring (Figure 2, Figures S1a and S1b in Supporting Information S1), the sediment at most sites remained similar over the long term after Hurricane Sally (Figures 9 and 10, Figures S4 and S6 in Supporting Information S1).

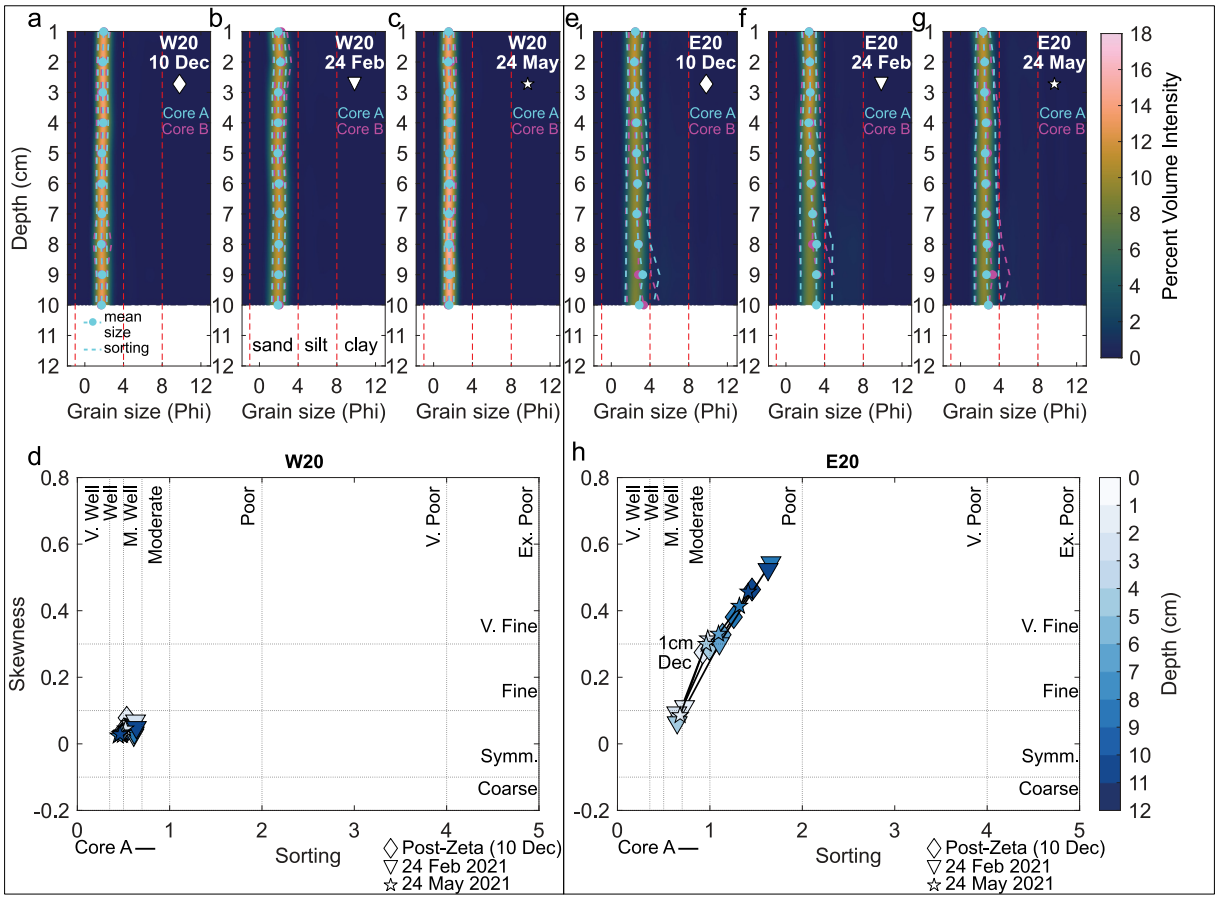

Figure 10. Profiles of grain size distribution (color gradient), mean grain size (φ; colored circles) and sorting (colored dashed lines) from (a), (e) after Hurricane Zeta to (b), (f) late February and (c), (g) late May at sites showing near-surface grain size changes consistent with winnowing of finer grains during Sally (a–d: W20 and e–h: E20). Grain size and sorting of replicate cores for which the color gradient is plotted are shown in cyan while other core is shown in magenta. "A" and "B" indicate replicate cores for a given site and time point. Color intensity reflects the percent volume of each grain size class for each layer. Vertical red dashed lines indicate sand, silt, and clay size class boundaries. Relationship of skewness and sorting for sites (d) W20 and (h) E20. Symbol colors correspond to sediment depth (only 1, 2, 4, 6, 8, and 10 cm depths shown). Shapes correspond to sampling time points in Figure 2.

4. Discussion

4.1. Potential Wave and Current Sediment Transport During Hurricane Sally

Hurricane Sally was the most intense storm event experienced by coastal Alabama in over a decade (Figures S2a–S2d in Supporting Information S1). Storm waves and currents generated bed shear stresses capable of transporting coarse sands at all sites for periods ranging from half a day to several days (Table 1, Figures 2b, 2d, 3a, 3c, and 3e; Nowell et al., 1981; Keen et al., 2006). Therefore, we expected to observe distinct storm beds resulting from substantial sediment resuspension and transport following passage of Hurricane Sally.

Past studies on extreme storm sediment transport have attributed offshore sediment transport and storm bed formation to storm surge ebb (e.g., Goff et al., 2010; Hayes, 1967), downwelling following storm-induced coastal setup (e.g., Cong et al., 2021; Morton, 1981; Snedden & Nummedal, 1991) or direct wind-driven transport (Gagan et al., 1990; Keen & Slingerland, 1993; Morton, 1981). Storm surge caused by Hurricane Sally only reached around 1 m in the study area, and Dauphin Island experienced little overwash and no channel cutting (Berg & Reinhart, 2021; Frank-Gilchrist et al., 2023). Bottom current measurements at CP also did not exhibit strong offshore currents after Sally that would be expected with substantial surge ebb (Figure 2d, Figures S1a, S1b, S1e, and S1f in Supporting Information S1; Dzwonkowski et al., 2022). In fact, the strong offshore winds from the northeast as Sally approached landfall caused a substantial drop in water level in Mobile Bay (Figure 2e; Berg & Reinhart, 2021). Relatively strong onshore flow occurred immediately after landfall (Figure 2d, Figures S1b and

S1d in Supporting Information S1; Dzwonkowski et al., 2022), indicating that sediment transport during Hurricane Sally likely did not occur via storm surge ebb.

The lack of strong offshore bottom currents and onshore surface currents after Hurricane Sally was also inconsistent with storm-driven coastal downwelling flow. During Hurricane Sally, current velocity measured at 20 m depth (CP) was almost constant in speed and direction throughout the entire water column and reached maximum velocity as Sally crossed the Alabama shelf (Figure 2d, Figures S1a–S1d in Supporting Information S1; Dzwonkowski et al., 2022). The overlapping surface and bottom boundary layers during Sally indicated the lack of geostrophic flow and has been observed and modeled at similar depths in other intense storms (Gagan et al., 1990; Keen & Slingerland, 1993; Morton, 1981). Therefore, most resuspension and sand transport in the study area that may have resulted from Hurricane Sally likely occurred during strong wind-driven westward currents as the storm crossed the shelf.

4.2. Spatially Variable Storm Beds Following Hurricane Sally

Because both current and wave-generated bed shear stresses were large (Figures 2d, 3a, 3c, and 3e, Figures S1a–S1d in Supporting Information S1), we expected both resuspension and transport during Hurricane Sally that would result in a discrete storm layer thinning with depth and distance away from the storm track (e.g., Goff et al., 2010; Hayes, 1967; Keen & Glenn, 2002). Ten days after Sally made landfall, however, evidence of hurricane impacts to surficial sediment structure varied considerably spatially along and across the Alabama shallow shelf. The sediments at the middle 12 and 20 m sites (Figure 1b) displayed sandy layers capped by a thin layer of finer and more poorly sorted sediment where muddier sediment had been present before Sally (M12) or was observed beneath the sand layer (M20; Figures 4i, 4j, 4n, 4o, 5b, and 5c, Figures S6 and S7 in Supporting Information S1), consistent with sand transport and deposition during Sally followed by finer sediment deposition after waves and currents waned following storm passage (e.g., Goff et al., 2010; Hayes, 1967). This apparent substantial sand deposition appeared to be confined to a small discrete area, as similar layers were not apparent at other sites. However, the coarsening and improved sorting of the top few centimeters of sediment observed at the western and eastern 20 m sites (W20 and E20) were consistent with fine sediment winnowing during Sally (e.g., Wheatcroft et al., 2007; Figures 4l, 4m, 4p, 4q, 5a, and 5d, Figure S7 in Supporting Information S1).

Grain size changes consistent with storm deposition and/or winnowing were not apparent at the remaining 5 and 12 m sites (Figure 4). The clean sands at the middle and eastern 5 m sites (M05 and E05) may have been resuspended and redeposited with little transport, had additional sand deposition, or been replenished by alongshore transport with sand eroded from the beach and/or shoreface from the east, resulting in no apparent net loss of sand from these sites (Keen et al., 2012; Mclaren, 1981). Given the strong near-bed currents observed at 20 m (CP) in addition to slight fining of M05 sands (Figures 2d, 4c, and 4d, Figure S4 in Supporting Information S1), sand replenishment from alongshore transport seemed more likely than resuspension with little sand movement at 5 m. Lidar bathymetry surveys shortly after Sally (late September-early October 2020) revealed additional evidence of sand transport, as 2.81×10^4 m^3 of sand was lost from a 183 m-long alongshore transect since 2018, which included the location of E05 (McGill et al., 2021). M05 was also located on the Mobile Bay ebb tidal delta and likely experienced frequent sand movement via tidal exchange (e.g., Hummel & Smith, 1996).

However, mean grain size at the western 5 m site (W05) became finer and more homogenous with depth but remained poorly sorted after Sally (Figures 4a and 4b, Figure S1 in Supporting Information S1). W05 was likely located in an erosive environment regardless of storm passage. The characteristic westward-directed longshore sand transport in the northern Gulf of Mexico is disrupted by the ebb tidal delta, including Sand Island, in addition to the dredged Mobile Bay shipping channel (Byrnes et al., 2013; Cipriani & Stone, 2001; Dzwonkowski et al., 2015), potentially creating a sand deficit just to the west of the ebb tidal delta (Morton, 2008; Otvos & Carter, 2008). Additionally, post-Sally Lidar bathymetry surveys showed a loss of 9.38×10^3 m^3 of sand along a 183 m-long transect near W05 since 2016 (McGill et al., 2021). Furthermore, cores collected near W05 in previous studies revealed thin (as little as <25 cm) shoreface sand layers overlying relict estuarine muddy sands and sandy muds deposited several thousand years ago during lower sea level (Hollis et al., 2019); this was consistent with the cores collected for this study, which displayed sand over grayish mud (Figure S5a in Supporting Information S1).

The sediments at W12 and E12 appeared to change little after Hurricane Sally (Figure 3, Figures S5b and S6 in Supporting Information S1). Although W12 is deeper than W05, westward sand transport to W12 during Sally

could have still been disrupted by the southward dip in bathymetry from the Mobile Bay ebb tidal delta that extends deeper than the 15 m isobath (e.g., Hummel, 1999, Figure 1). Dzwonkowski and Park (2012) demonstrated that seasonally averaged spring and summer along-shelf flow on the Alabama coast is likely deflected offshore at the ebb tidal delta due in part to flow separation around the dip in bathymetry. The momentum of the strong west-southwestward flow during Sally may have also carried sediment offshore at the ebb tidal delta, preventing sand delivery to the western sites. Flow diversion by seafloor bathymetric features such as sand ridges can enhance local sediment accumulation (Hayes, 1967), which may have occurred at the ebb tidal delta and concentrated sand transport to sites M12 and M20, resulting in these sites displaying sand layers that the eastern 12 and 20 m sites lacked despite being closer to the hurricane track (Figures 1b and 3). Furthermore, another likely reason for the lack of consistent sand bed deposition across these sites is the generally low sand availability for Dauphin Island and Fort Morgan (Anderson et al., 2023; Hollis et al., 2019; Otvos & Carter, 2013).

4.3. Minor Impacts of Hurricane Zeta on Sediment and Hurricane Sally Storm Beds

Difficulties in interpreting ancient storm beds have been attributed to post-depositional alteration processes, including subsequent storms, which may completely or partially erode or incorporate previous storm beds into new ones (Goni et al., 2007; Keen et al., 2012; Wheatcroft et al., 2007; Xu et al., 2016). Hurricane Zeta impacted the study area only 6 weeks after Hurricane Sally, allowing a rare and direct observation of subsequent storm impacts to recently deposited storm beds (e.g., Allison et al., 2005; Goni et al., 2007). Despite making landfall several hundred kilometers to the southwest of the study area, Zeta still generated strong winds and the second highest significant wave heights recorded off the Alabama coast in over a decade (Table 1, Figures 1c, 2a, and 2b, Figure S2b in Supporting Information S1). In contrast to days of high wave shear stress before and after Sally, elevated wave shear stress during Zeta only lasted a few hours at most sites, and current shear stress was likely much lower relative to Sally (Table 1, Figures 3b, 3d, and 3f, Figures S1a and S1b in Supporting Information S1). Additionally, storm surge and post-hurricane river discharge was higher than during Sally due to higher rainfall generated within the Mobile Bay watershed during Zeta (Figures 2d, 2e, and 2f, Figures S1e and S1f in Supporting Information S1; Blake et al., 2021), suggesting storm beds produced by Zeta would differ substantially from post-Sally beds.

Post-Zeta sampling took place ∼1.5 months after landfall, during which there were several periods of high winds and waves (Figures 2a and 2b), making it difficult to attribute the sediment structure observed in December directly to Zeta. However, the relatively small changes in surficial sediment structure (especially at 12 and 20 m sites) suggest a lack of significant alteration of potential storm beds produced by Sally during Zeta (Figures 6a, 6b, 6e, 6f, 7, and 8, Figures S4, S6, and S7 in Supporting Information S1). This emphasizes the importance of strong currents for generation of thick storm beds demonstrated by modeling studies (e.g., Bentley et al., 2002; Cong et al., 2021; Keen & Glenn, 2002; Snedden & Nummedal, 1991) and suggests that storm beds may be preserved even from subsequent extreme storms if those storms lack strong bottom currents.

4.4. Long-Term Sediment Changes in Absence of Hurricanes

The potential impacts of Hurricane Sally on Alabama shallow shelf sediments observed at 12 and 20 m depths appeared to withstand post-depositional reworking by Hurricane Zeta, but the putative storm layers could face more gradual erosion by less-extreme waves and currents as well as bioturbation over longer time scales (years to decades; Keen et al., 2012; Bentley & Nittrouer, 2012). Over the winter, despite strong north winds that generated relatively high waves and currents (Figures 2a, 2b, and 2d, Figures S1a and S1b in Supporting Information S1), sediment composition at most sites changed little apart from shifts in sand layer thicknesses that could have resulted from erosion and deposition or spatial variability (Figures 6f, 6g, 9a, 9b, 9d, 10, Figures S4, S6, and S7 in Supporting Information S1). The sediment at sites W05 and M20, however, appeared to change between December and late February, exhibiting increased mud content and heterogeneity between cores (Figures 6b, 6c, 9e, 9f, and 9h, Figures S4 and S7 in Supporting Information S1).

In addition to generating waves and currents, the strong winter winds likely resuspended and transported large amounts of mud from Mobile Bay offshore, along with mud transported by elevated river discharge during the winter (Figures 2e and 2f; Dinnel et al., 1990). Satellite imagery taken shortly after periods of high wind and/or river discharge during the winter and spring showed mostly southward and/or westward sediment plumes exiting Mobile Bay, which may have been responsible for increased mud at W05 and M20 (Figures S8a–S8d in

Supporting Information S1; e.g., Gagan et al., 1990; Bentley et al., 2002). However, muddy sediment transported out of Mobile Bay in surface plumes is mostly deposited offshore in deeper water (Dinnel et al., 1990; Hummell, 1996), making it unlikely that the mud increase in most of the top 10 cm of sediment at W05 was due solely to sediment plume delivery (Figure 6c, Figures S4a–S4g in Supporting Information S1). Furthermore, while W12 sediments could have received plume-derived sediment and not shown much change in composition, there was no evidence of mud deposition at sites M12 or W20 despite their proximity to sediment plumes observed over the winter (Figures 9b, 9d, 10b, and 10d, Figures S6, S7, and S8a–S8d in Supporting Information S1). Instead, the muddier sediment at W05 was more consistent with erosion into the relict estuarine muds found in earlier cores (Hollis et al., 2019). Additionally, the muddy layer at M20 was only observed in one core and may have simply reflected small-scale spatial variability.

Strong winds continued to impact the study area while river discharge into Mobile Bay peaked over the spring (Figures 2a–2e, and 2f), but by late May, the sediment at most sites displayed few substantial changes. Sandy layers became slightly thinner (E20) or thicker (M12). The surface mud layer observed at M20 in late February was absent in May (Figures 9, 10f, 10g, and 10h, Figures S6 and S7 in Supporting Information S1), which was surprising given that there was elevated river discharge and large sediment plumes visible via satellite in early April (Figures 2e and 2f, Figures S8f–S8h in Supporting Information S1). However, the high waves and near-bed currents during the uncharacteristically windy 5-day period in mid-May could have winnowed a potential surface mud layer (Figure 2). W05 sediments became sandier but remained muddy, poorly sorted, and finely skewed, resembling the deep mud layer observed in pre-Sally cores (Figures 6c and 6d, Figures S4 and S5a in Supporting Information S1), suggesting the relict estuarine sediments that were potentially eroded into over the winter remained at the surface or continued to be eroded over the spring (Hollis et al., 2019). E12 was the only site in which the sediment composition changed dramatically between late February and late May, shifting from sand over muddy sand to organic-rich silts (Figures 6g and 6h, Figures S6o–S6u in Supporting Information S1). Based on the thickness of the mud (exceeding 30 cm in some cores) and sediment plumes predominantly oriented westward or southwestward during the spring (Figures S8e–S8h in Supporting Information S1), this mud increase was not likely a result of mud directly transported out of Mobile Bay. Instead, E12 may have been close to or within a muddier patch surrounded by sandier sediments south of Ft. Morgan that has been shown to vary spatially and temporally (Hummel, 1999, Figures 11 and 12). In general, there was likely resuspension of shoreface sediments (i.e., 5 m sites) over the winter and spring while deeper sites showed little impact of the strong winds and/or offshore mud transport out of Mobile Bay observed over this period.

The sedimentary changes attributed to Hurricane Sally appeared to remain relatively stable out to 8 months after Sally. While Sally did not appear to generate extensive storm beds in comparison to tropical cyclones in other studies (e.g., Allison et al., 2005; Bentley et al., 2002; Cong et al., 2021; Hayes, 1967), the observed storm-induced sediment changes, especially at 20 m sites, appeared to resist substantial alteration by Hurricane Zeta in addition to the strong winds and offshore mud transport over the winter and spring (Figures 2, 3, 7, 8, 9, and 10, Figures S7 and S8 in Supporting Information S1).

4.5. Capturing Spatial Variability of Storm Impacts to Sediment Structure

Directly sampling sediment changes and storm hydrodynamics close in time and space to unpredictable and destructive extreme storm events is challenging (Corbett et al., 2014; Xu et al., 2016), and modeling allows assessment of storm impacts for which high-resolution sampling proximal to and immediately before and after a storm impact is unavailable (Bentley et al., 2002; Cong et al., 2021; Keen & Slingerland, 1993; Xu et al., 2016). This study, however, demonstrates the benefits of coastal hydrological monitoring in addition to opportunistic pre- and post-storm sediment sampling. Sediment sampling over a relatively large area (<500 km^2) and continuous current measurements (Figure 2d, Figure S1 in Supporting Information S1; Dzwonkowski & Lockridge, 2021; Dzwonkowski et al., 2022) captured spatial variability in post-storm sediment changes that were consistent with the offshore deflection of storm-generated sand transport by the Mobile Bay ebb tidal delta, resulting in sand deposition in a narrow offshore area (Figures 1b and 3, Figures S6 and S7 in Supporting Information S1). These results demonstrate the importance of sediment sampling to account for storm current interactions with bathymetry. For systems with low sand supply, storm signals in the sediment may be overlooked if sampling is too broad; especially in areas to the right of storm passage that experience less intense physical forcing than to the left in the northern hemisphere (e.g., Cong et al., 2021). Along storm-prone coasts, the combination of hydrographic monitoring and high temporal resolution, spatially variable sampling will become

more important for assessing and predicting storm impacts to coastal sediment dynamics, especially with the predicted increase in rapid intensification of storms expected with climate change (Emanuel, 2017).

5. Conclusion

Hurricane Sally was the most intense storm to impact coastal Alabama in over a decade and coincided with spatially heterogenous changes to inner shelf surficial sediment composition. After Sally, the potential concentration of sand delivery at some sites and lack of noticeable hurricane impacts at others was consistent with high wave and current energy and differences in depth, low sand supply, pre-storm sediment type and location relative to bathymetric features (i.e., the Mobile Bay ebb tidal delta). In the 8 months after Sally, the sand layers and near-surface fine sediment winnowing attributed to Sally remained relatively stable despite the proximal impact of Hurricane Zeta in addition to strong winds and sediment plumes during the winter and spring. This study emphasizes the importance of sampling to account for spatial variability in storm impacts, especially on river-influenced coasts, as well as understanding how storm flow interacts with local bathymetry and contributes to post-storm deposition. Understanding these variable storm impacts to dynamic river-influenced coastal sediments will be especially important for predicting coastal sediment transport as climate change leads to increased intensity of extreme storms.

Data Availability Statement

Data from the NOAA National Data Buoy Center stations 42012, DPIA1, and BCKA1 (https://www.ndbc.noaa.gov/), USGS Station 02470629 (https://waterdata.usgs.gov/monitoring-location/02470629/), the Fisheries Oceanography in Coastal Alabama (FOCAL) acoustic doppler wave and current profiler mooring (Dzwonkowski & Lockridge, 2021), and ADCIRC wave height hindcast data from the Coastal Emergency Risk Assessment (CERA) website (http://cera.coastalrisk.live/) were used in the creation of this manuscript. Satellite images were obtained from the University of Florida's Optical Oceanography Laboratory (https://optics.marine.usf.edu/cgi-bin/optics_data?roi=MBAY&current=1). Sediment property and grain size distribution data presented in this manuscript have been submitted to the National Science Foundation Biological and Chemical Oceanography Data Management Office and are available under the project CAREER: Mechanisms of bioturbation and ecosystem engineering by benthic infauna (Clemo & Dorgan, 2023; https://www.bco-dmo.org/dataset/916071). Figures were made with Matlab Version R2023b, Google Earth Pro, and Affinity Designer.

Acknowledgments

This work was funded by NSF grant CAREER OCE #1844910. In addition, this paper is a result of research funded by the National Oceanic and Atmospheric Administration's RESTORE Science Program under award NA19NOS4510194 to the University of South Alabama and the Integrated Ocean Observing System via the Gulf of Mexico Coastal Ocean Observing System (GCOOS). We thank Madeline Frey, Samir Sirk Morató, Moey Rojas, Jennifer Duncan, Elizabeth Byrd, Riann Martin, and Chesna Cox for sediment processing and Grant Lockridge, Matthew Boehm, Josh Goff, William Ballentine, Kara Gadeken, Cassandra Bates, and Jesse Gwinn for core collection, and DISL captains Jonathan Wittmann, Diana Marchant, and Michael Daudt. We also thank Zhilong Liu for generating wind field maps in Figure 1 and Shara Gremillion for providing Matlab scripts for plotting grain size distribution profiles. The authors declare no conflicts of interest.

References

Allison, M. A., Sheremet, A., Goni, M. A., & Stone, G. W. (2005). Storm layer deposition on the Mississippi–Atchafalaya subaqueous delta generated by Hurricane Lili in 2002. *Continental Shelf Research*, *25*(18), 2213–2232. https://doi.org/10.1016/j.csr.2005.08.023

Anderson, J. B., Wallace, D. J., Rodriguez, A. B., & Simms, A. R. (2023). Unprecedented historical erosion of U.S. Gulf coast: A consequence of accelerated sea-level rise? *Earth's Future*, *11*(9), e2023EF003676. https://doi.org/10.1029/2023EF003676

Anderson, J. B., Wallace, D. J., Rodriguez, A. B., Simms, A. R., & Milliken, K. T. (2022). Holocene evolution of the western Louisiana-Texas coast, USA: Response to sea-level rise and climate change. *Geological Society of America Memoir*, *221*, 1–81.

Balsam, W. L., & Beeson, J. P. (2003). Sea-floor sediment distribution in the Gulf of Mexico. *Deep-Sea Research I*, *50*(12), 1421–1444. https://doi.org/10.1016/j.dsr.2003.06.001

Bentley, S. J., Keen, T. R., Ann, C., & Vaughan, W. C. (2002). The origin and preservation of a major hurricane event bed in the northern Gulf of Mexico: Hurricane Camille, 1969. *Marine Geology*, *186*(3–4), 423–446. https://doi.org/10.1016/s0025-3227(02)00297-9

Bentley, S. J., & Nittrouer, C. A. (2012). Accumulation and intense bioturbation of bioclastic muds along a carbonate-platform margin: Dry Tortugas, Florida. *Marine Geology*, *315–318*, 44–57. https://doi.org/10.1016/j.margeo.2012.05.002

Berg, R., & Reinhart, B. J. (2021). *Hurricane sally (AL192020): 11-17 Septemeber 2020* (pp. 1–69). National Hurricane Center Tropical Cyclone Report, National Hurricane Center.

Blake, E., Berg, R., & Hagen, A. (2021). National hurricane center tropical cyclone report: Hurricane Zeta (AL282020).

Blott, S. J., & Pye, K. (2001). Gradistat: A grain size distribution and statistics package for the analysis of unconsolidated sediments. *Earth Surface Processes and Landforms*, *26*(11), 1237–1248. https://doi.org/10.1002/esp.261

Boudreau, B. P. (1998). Mean mixed depth of sediments: The wherefore and the why. *Limnology & Oceanography*, *43*(3), 524–526. https://doi.org/10.4319/lo.1998.43.3.0524

Boudreau, B. P., & Jorgensen, B. B. (Eds.) (2001). *The benthic boundary layer: Transport processes and biogeochemistry*.

Brutsché, K. E., Rosati, J., Pollock, C. E., & Mcfall, B. C. (2016). *Calculating depth of closure using WIS hindcast data* (Vol. 1–9). US Army Corps of Engineers.

Byrnes, M. R., Berlinghoff, J. L., & Griffee, S. F. (2017). *Regional sediment dynamics in Mobile Bay, Alabama; a sediment budget perspective* (Vol. 1–9). US Army Corps of Engineers.

Byrnes, M. R., Rosati, J. D., Griffee, S. F., & Berlinghoff, J. L. (2013). Historical sediment transport pathways and quantities for determining an operational sediment budget: Mississippi sound barrier islands. *Journal of Coastal Research*, *SI*(63), 166–183. https://doi.org/10.2112/SI63-014.1

Cipriani, L. E., & Stone, G. W. (2001). Net longshore sediment transport and textural changes in beach sediments along the southwest Alabama and Mississippi barrier islands, U.S.A. *Journal of Coastal Research*, *17*(2), 443–458.
Clemo, W. C., & Dorgan, K. M. (2023). Sediment properties collected off the Alabama coast before and after Hurricane Sally, 2020-2021. *Biological and Chemical Oceanography Data Management Office (BCO-DMO)*. https://doi.org/10.26008/1912/bco-dmo.916071.1
Clemo, W. C., Dorgan, K. M., Wallace, D. J., & Dzwonkowski, B. (2023). Effects of Hurricane Sally (2020) On Sediment Structure and Infaunal Communities In Coastal Alabama. In *Coastal sediments 2023: The proceedings of the coastal sediments 2023* (pp. 1055–1068).
Cong, S., Wu, X., Ge, J., Bi, N., Li, Y., Lu, J., & Wang, H. (2021). Impact of Typhoon Chan-hom on sediment dynamics and morphological changes on the East China Sea inner shelf. *Marine Geology*, *440*(May), 106578. https://doi.org/10.1016/j.margeo.2021.106578
Corbett, D. R., Walsh, J. P., Harris, C. K., Ogston, A. S., & Orpin, A. R. (2014). Formation and preservation of sedimentary strata from coastal events: Insights from measurements and modeling. *Continental Shelf Research*, *86*, 1–5. https://doi.org/10.1016/j.csr.2014.06.011
Dinnel, S. P., Schroeder, W. W., & Wiseman, W. J. (1990). Estuarine-shelf exchange using Landsat images of discharge plumes. *Journal of Coastal Research*, *6*(4), 789–799.
DuVal, C. B., Trembanis, A. C., & Miller, D. C. (2021). A regime-state framework for morphodynamic modeling of seabed roughness. *Journal of Geophysical Research: Oceans*, *126*(5), 1–26. https://doi.org/10.1029/2020JC016769
Dzwonkowski, B., Fournier, S., Lockridge, G., Coogan, J., Liu, Z., & Park, K. (2021). Cascading weather events amplify the coastal thermal conditions prior to the shelf transit of Hurricane Sally (2020). *Journal of Geophysical Research: Oceans*, *126*(12). https://doi.org/10.1029/2021JC017957
Dzwonkowski, B., Fournier, S., Lockridge, G., Coogan, J., Liu, Z., & Park, K. (2022). Hurricane Sally (2020) shifts the ocean thermal structure across the inner core during rapid intensification over the shelf. *Journal of Physical Oceanography*, *52*(11), 2841–2852. https://doi.org/10.1175/jpo-d-22-0025.1
Dzwonkowski, B., & Lockridge, G. (2021). Fisheries Oceanography in Coastal Alabama (FOCAL) acoustic doppler wave and current profiler data from 2020-08-05 to 2021-06-03 (NCEI Accession 0241013) [Dataset]. *NOAA National Centers for Environmental Information*. https://doi.org/10.25921/92x0-fy55
Dzwonkowski, B., & Park, K. (2012). Subtidal circulation on the Alabama shelf during the Deepwater Horizon oil spill. *Journal of Geophysical Research*, *117*(C3), 1–15. https://doi.org/10.1029/2011JC007664
Dzwonkowski, B., Park, K., & Collini, R. (2015). The coupled estuarine-shelf response of a river-dominated system during the transition from low to high discharge. *Journal of Geophysical Research: Oceans*, *120*(9), 6145–6163. https://doi.org/10.1002/2015JC010714.Received
Dzwonkowski, B., Park, K., Kyung, H., Graham, W. M., Hernandez, F. J., & Powers, S. P. (2011). Hydrographic variability on a coastal shelf directly influenced by estuarine outflow. *Continental Shelf Research*, *31*(9), 939–950. https://doi.org/10.1016/j.csr.2011.03.001
Emanuel, K. (2017). Will global warming make hurricane forecasting more difficult? *Bulletin of the American Meteorological Society*, *98*(3), 495–502. https://doi.org/10.1175/BAMS-D-16-0134.1
FitzGerald, D. M., Fenster, M. S., Argow, B. A., & Buynevich, I. V. (2008). Coastal impacts due to sea-level rise. *Annual Review of Earth and Planetary Sciences*, *36*(1), 601–647. https://doi.org/10.1146/annurev.earth.35.031306.140139
Folk, R. L., & Ward, W. C. (1957). Brazos River Bar: A study in the significance of grain size parameters. *Journal of Sedimentary Research*, *27*(1), 3–26. https://doi.org/10.1306/74d70646-2b21-11d7-8648000102c1865d
Frank-Gilchrist, D. P., Passeri, D. L., & Bilskie, M. V. (2023). Hindcast of Hurricane Sally impacts on barrier islands in the Gulf of Mexico. In *Coastal sediments 2023: The proceedings of the coastal sediments 2023* (pp. 2220–2227).
Gagan, M. K., Chivas, A. R., & Herczeg, A. L. (1990). Shelf-wide erosion, deposition, and suspended sediment transport during cyclone Winifred, central Great Barrier Reef, Australia. *Journal of Sedimentary Petrology*, *60*(3), 456–470. https://doi.org/10.1306/212F91BF-2B24-11D7-8648000102C1865D
Goff, J. A., Allison, M. A., & Gulick, S. P. S. (2010). Offshore transport of sediment during cyclonic storms: Hurricane Ike (2008), Texas Gulf Coast, USA. *Geological Society of America*, *38*(4), 351–354. https://doi.org/10.1130/G30632.1
Goni, M. A., Alleau, Y., Corbett, R., Walsh, J. P., Mallinson, D., Allison, M. A., et al. (2007). The effects of Hurricanes Katrina and Rita on the seabed of the Louisiana Shelf. *The Sedimentary Record*, *5*(1), 4–9. https://doi.org/10.2110/sedred.2007.1.4
Hayes, M. O. (1967). Hurricanes as geological agents: Case studies of Hurricanes Carla, 1961, and Cindy, 1963. *The University of Texas at Austin Bureau of Economic Geology Report of Investigations*, *61*, 1–54. https://doi.org/10.23867/ri0061d
Hollis, R. J., Wallace, D. J., Miner, M. D., Gal, N. S., Dike, C., & Flocks, J. G. (2019). Late Quaternary evolution and stratigraphic framework in fluence on coastal systems along the north-central Gulf of Mexico, USA. *Quaternary Science Reviews*, *223*, 105910. https://doi.org/10.1016/j.quascirev.2019.105910
Hummel, R. L. (1999). *Geologic and economic characterization and near-term potential of sand resources of the east Alabama inner continental shelf offshore of Morgan Peninsula*. Geological Survey of Alabama.
Hummel, R. L., & Smith, W. E. (1996). *Geological resource delineation and hydrographic characterization of an offshore sand resource site for use in beach nourishment projects on Dauphin*. Island.
Hummell, R. L. (1996). Holocene geologic history of coastal Alabama.
Jackson, D. R., & Richardson, M. D. (2007). *High-frequency seafloor acoustics*. Springer. https://doi.org/10.1016/0041-624X(71)90393-3
Jacquot, M. P., Dorgan, K. M., Mortazavi, B., Kleinhuizen, A. A., & Clemo, W. C. (2018). Macrobenthic community structure and influence on denitrification capacity in soft sediments (Mobile Bay, Alabama, USA). *Marine Ecology Progress Series*, *605*, 17–35. https://doi.org/10.3354/meps12759
Jenkins, C. (2011). Seabed Sediment Folk Codes In Gulf of Mexico Data Atlas. [Internet]. *Stennis Space Center (MS): National Centers for Environmental Information*. https://gulfatlas.noaa.gov/
Jumars, P. A., & Nowell, A. R. M. (1984). Fluid and sediment dynamic effects on marine benthic community structure. *American Zoology*, *24*(1), 45–55. https://doi.org/10.1093/icb/24.1.45
Keen, T. R., Furukawa, Y., Bentley, S. J., Slingerland, R. L., Teague, W. J., Dykes, J. D., & Rowley, C. D. (2006). Geological and oceanographic perspectives on event bed formation during Hurricane Katrina. *Geophysical Research Letters*, *33*(23), 1–5. https://doi.org/10.1029/2006GL027981
Keen, T. R., & Glenn, S. M. (2002). Predicting bed scour on the continental shelf during Hurricane Andrew. *Journal of Waterway, Port, Coastal, and Ocean Engineering*, *128*(6), 249–258. https://doi.org/10.1061/(asce)0733-950x(2002)128:6(249)
Keen, T. R., & Slingerland, R. L. (1993). A numerical study of sediment transport and event bed genesis during Tropical Storm Delia. *Journal of Geophysical Research*, *98*(3), 4775–4791. https://doi.org/10.1029/92jc02757
Keen, T. R., Slingerland, R. L., Bentley, S. J., Furukawa, Y., Teague, W. J., & Dykes, J. D. (2012). Sediment transport on continental shelves: Storm bed formation and preservation in heterogeneous sediments. *International Association of the Sedimentologists Special Publications*, *44*, 295–310. https://doi.org/10.1002/9781118311172.ch14

Li, Y., Li, H., Qiao, L., Xu, Y., Yin, X., & He, J. (2015). Storm deposition layer on the Fujian coast generated by Typhoon Saola (2012). *Scientific Reports*, *5*(1), 14904. https://doi.org/10.1038/srep14904

McGill, S., Sylvester, C., Dunkin, L., Eisemann, E., & Wozencraft, J. (2021). 2020 hurricane impact assessment for the northern Gulf of Mexico: Hurricane Sally and Hurricane Zeta. *Shore and Beach*, *89*(2), 1–9. https://doi.org/10.34237/1008927

Mclaren, P. (1981). An interpretation of trends in grain size measures. *Journal of Sedimentary Petrology*, *51*(2), 611–624.

Meysman, F. J. R., Middelburg, J. J., & Heip, C. H. R. (2006). Bioturbation: A fresh look at Darwin's last idea. *Trends in Ecology & Evolution*, *21*(12), 688–695. https://doi.org/10.1016/j.tree.2006.08.002

Morton, R. A. (1981). Formation of storm deposits by wind-forced currents in the Gulf of Mexico and the North Sea. *Special Publications of the International Association of Sedimentologists*, *5*, 385–396. https://doi.org/10.1002/9781444303759.ch27

Morton, R. A. (1988). Near shore responses to great storms. *Geological Society of America*, *229*, 7–22. https://doi.org/10.1130/spe229-p7

Morton, R. A. (2008). Historical changes in the Mississippi-Alabama barrier-island chain and the roles of extreme storms, sea level, and human activities. *Journal of Coastal Research*, *24*(6), 1587–1600. https://doi.org/10.2112/07-0953.1

Nowell, A. R. M., Jumars, P. A., & Eckman, J. E. (1981). Effects of biological activity on the entrainment of marine sediments. *Marine Geology*, *42*(1–4), 133–153. https://doi.org/10.1016/0025-3227(81)90161-4

Otvos, E. G., & Carter, G. A. (2008). Hurricane degradation-barrier development cycles, northeastern Gulf of Mexico: Landform evolution and island chain history. *Journal of Coastal Research*, *24*(2), 463–478. https://doi.org/10.2112/06-0820.1

Otvos, E. G., & Carter, G. A. (2013). Regressive and transgressive barrier islands on the North-Central Gulf Coast-Contrasts in evolution, sediment delivery, and island vulnerability. *Geomorphology*, *198*, 1–19. https://doi.org/10.1016/j.geomorph.2013.05.015

Snedden, J. W., & Nummedal, D. (1991). Origin and geometry of storm-deposited sand beds in modern sediments of the Texas continental shelf. *Special Publications of the International Association of Sedimentologists*, *14*, 283–308. https://doi.org/10.1002/9781444303933.ch8

Solan, M., Ward, E. R., White, E. L., Hibberd, E. E., Cassidy, C., Schuster, J. M., et al. (2019). Worldwide measurements of bioturbation intensity, ventilation rate, and the mixing depth of marine sediments. *Scientific Data*, *6*(1), 1–6. https://doi.org/10.1038/S51597-019-0069-7

Stumpf, R. P., Gelfenbaum, G., & Pennock, J. R. (1993). Wind and tidal forcing of a buoyant plume, Mobile Bay, Alabama. *Continental Shelf Research*, *13*(11), 1281–1301. https://doi.org/10.1016/0278-4343(93)90053-z

Wallace, D. J., & Anderson, J. B. (2013). Unprecedented erosion of the upper texas coast: Response to accelerated sea-level rise and hurricane impacts. *Bulletin of the Geological Society of America*, *125*(5–6), 728–740. https://doi.org/10.1130/B30725.1

Wheatcroft, R. A., Wiberg, P. L., Alexander, C. R., Bentley, S. J., Drake, D. E., Harris, C. K., & Ogston, A. S. (2007). Post-depositional alteration and preservation of sedimentary strata. *Continental Margin Sedimentation: From Sediment Transport to Sequence Stratigraphy*, *37*, 101–155.

Wiberg, P. L., & Sherwood, C. R. (2008). Calculating wave-generated bottom orbital velocities from surface-wave parameters. *Computers & Geosciences*, *34*(10), 1243–1262. https://doi.org/10.1016/j.cageo.2008.02.010

Xu, K., Mickey, R. C., Chen, Q., Harris, C. K., Hetland, R. D., Hu, K., & Wang, J. (2016). Computers and Geosciences Shelf sediment transport during hurricanes Katrina and Rita. *Computers & Geosciences*, *90*, 24–39. https://doi.org/10.1016/j.cageo.2015.10.009